COVER LETTER

Manuscript ID: acp-2020-60

Dear Editor,

We would like to thank you for giving us the opportunity to revise our manuscript, now titled "Aerosol solar radiative forcing near the Taklimakan Desert based on radiative transfer and regional meteorological simulations during the Dust Aerosol Observation-Kashi campaign". We appreciate the reviewers for thoughtful review of previous manuscript. They raised important issues and the comments are very helpful to improve the manuscript. We have carefully taken these comments into consideration and have revised our manuscript accordingly. The changes within the manuscript were highlighted using red text in the red-lined version. We are confident that the new version of the manuscript is significantly improved.

We respond in detail to each of the reviewers' comments in the author response files. Please find the reviewers' comments repeated in blue italics, and followed by our responses in black and revisions in bold. We hope that the reviewers will find our responses to their comments satisfactory.

Thanks for all the help!

Sincerely,

Li Li

lili3@radi.ac.cn

To Anonymous Reviewer #1: (Comment ID:acp-2020-60-RC1)

Dear Reviewer,

Thank you very much for carefully reviewing our manuscript. The constructive and thoughtful comments have helped us a lot to improve the paper. Following these suggestions, we have taken a lot of efforts to optimize the structure and to make the writing more concise and clear. Please find below the comments in blue italics and our responses in black and the changes in bold.

Responses to general comments:

In this manuscript, the measurements obtained during the Dust Aerosol Observation-Kashi campaign were employed in radiative transfer model and the estimations were improved by considering the actual measured atmospheric profiles and diurnal variations of land surface albedo. Direct aerosol solar radiative forcing of dust aerosols was analyzed based on comprehensive parameters and numerical models. The effects of data assimilations on estimating the radiative forcing effects were also explored. However, the manuscript was poorly worded, thus making me confused. The manuscript needs to structure writing accurately to produce proper paragraphs with clear topics. Major revisions are necessary before the manuscript is finally accepted for publication.

Reply: We thank the reviewer for the constructive criticisms that have helped us to improve our manuscript. We have worked hard on optimizing the structure of the manuscript. In the revised manuscript, we reorganized some sections:

1) subsection **"2.1 Experimental site and instrumentation" was divided into "2.1 Observation site" and "2.2 Instrumentation"**;

2) subsection **"2.2 Aerosol properties during the DAO-K campaign" was incorporated into subsection " 4.1 Aerosol solar radiative forcing and efficiency"**;

3) subsection **"3.3.3 Experimental setup" was rephrased as "3.3.3 Model setup"** to avoid confuse with the subsection of " Instrumentation";

4) section **"4 Results and Discussion" was changed to "4 Results of radiative transfer simulations"**;

5) subsection **"4.3 Comparisons and validation" was isolated from section 4 and changed to "5 Comparison with WRF-Chem simulations"** to avoid too much contents in section 4;

6) subsection **"4.3.1 Comparison between radiative transfer simulations and AERONET results" was renamed as "4.3 Difference from AERONET products"**, and was moved to follow the section 4.2 to state and discuss the results of radiative transfer model simulations together.

The new structure contains 6 parts: 1) Section "1 Introduction" begins with the introduction of background and significance, current status and problems, as well as research mentality and content of this manuscript. 2) Section "2 Dust Aerosol Observation-Kashi field campaign" gives a brief introduction of the DAO-K field campaign, and an overview of the multi-source observations and data. 3) Section "3 Estimation of aerosol solar radiative forcing" describes the methods to estimate *ASRF* by improving the inputs of atmospheric profiles and land surface albedo in RT simulation, and by employing data assimilation in the WRF-Chem simulation. 4) Section "4 Results of radiative transfer simulations" presents the results of *ASRF* simulated by RT model during the field campaign and for some specific cases. The influences of the atmosphere and surface conditions on the results are discussed. The difference from the corresponding AERONET operational products are also analyzed. 5) Section "5 Comparison with WRF-Chem simulations" gives direct comparison between the RT and WRF-Chem model simulations. Both the model simulations are evaluated based on the simultaneous irradiance measurements. 6) "Summary and conclusions" are given in Section 6. We believe that the new structure is more concise and understandable. We hope our revisions have satisfactorily addressed these issues.

Responses to specific comments:

1. Section 1, this part should introduce the research background and significance, current status, concealed problems, as well as research mentality and content of this manuscript. Nevertheless, the introduction of this manuscript is inundated with accumulation of literatures rather than sublimation of these research results. The authors need survey more literatures in recent five years and then summarized them.

Reply: Thank you for the frank comments and helpful suggestions. Following the suggestions, we have spent a lot of time to review and summarize related literatures. And on that basis we

restructured the "introduction" section and clarify the research background and significance, current status, concealed problems, as well as research mentality and content of this study. We have made a number of changes in these respects. Major revisions concentrated in the second and third paragraphs:

"**As one of the largest sandy deserts in the world, the Taklimakan Desert located in the Xinjiang Uygur Autonomous Region of China is a main source region of Asian dust (Huang et al., 2009), which influences not only surrounding areas such as the Tibetan Plateau (Liu et al., 2008; Chen et al., 2013; Yuan et al., 2019), but also wide regions in Eastern Asia (Mikami et al., 2006; Liu et al., 2011b; Yuan et al., 2019), even North America and Greenland through long-range transports across the Pacific Ocean (Bory et al., 2003; Chen et al., 2017; Liu et al., 2019). An accurate assessment of the Taklimakan aerosol solar radiative forcing (*ASRF*, defined as the difference of the net solar irradiance with and without aerosols presence) is important to evaluate regional and global climate changes. However, simulations by different models with different observation inputs varied widely in literatures. Huang et al. (2009) employed the Fu-Liou RT model to simulate the Taklimakan *ASRF* during the dust episodes in the summer of 2006, and reported that the dust particles result in average daily mean SW warming of 14 W m^{-2} at the top of atmosphere (TOA), atmospheric warming of 79 W m^{-2}, and surface cooling of -65 W m^{-2}. Sun et al. (2012) adopted the RegCM4 simulations and reported both negative *ASRF* (i.e., cooling effects) of dust particles at the TOA and bottom of atmosphere (BOA) with the strongest values in spring during 2000~2009 period, reaching up to -4 W m^{-2} and -25 W m^{-2} in the Taklimakan Desert region, respectively. Li et al. (2018) also reported the negative multi-year average SW aerosol radiative forcing of -16 W m^{-2} at the TOA and -18 W m^{-2} at the BOA at the edge of Taklimakan Desert, Kashi station based on the SBDART simulations. The simulated results of dust aerosol radiative forcing have rarely been confirmed, especially in the Taklimakan Desert (Xia et al., 2009). Performances of various models sometimes were evaluated against the observations of aerosol optical depth (*AOD*), aerosol extinction profile, single scattering albedo (*SSA*), and particle size distribution (Zhao et al., 2010; Chen et al., 2014). Nevertheless, comparison of irradiance is indispensable to provide direct evidence for corroborating the *ASRF* simulated results.**"

"**An intensive dust field campaign is essential for comprehensive investigating the optical, physical, chemical, and radiative properties of dust aerosol particles over Taklimakan Desert. As such, one of the goals of the Dust Aerosol Observation-Kashi (DAO-K) field campaign is to provide high quality dataset on aerosol in this region to obtain accurate assessment of the Taklimakan aerosol solar radiative forcing…**"

Please find them in the section "1 Introduction" in the revised manuscript.

References:

Bory, A. J., Biscaye, P. E., and Grousset, F. E.: Two distinct seasonal Asian source regions for mineral dust deposited in Greenland (NorthGRIP), Geophys. Res. Lett., 30, 1167, doi:10.1029/2002GL016446, 2003.

Chen, S., Huang, J., Zhao, C., Qian, Y., Leung, L. R., and Yang, B.: Modeling the transport and radiative forcing of Taklimakan dust over the Tibetan Plateau: A case study in the summer of 2006, J. Geophys. Res. Atmos., 118, 797-812, doi:10.1002/jgrd.50122, 2013.

Chen, S., Zhao, C., Qian, Y., Leung, L. R., Huang, J., Huang, Z., Bi, J., Zhang, Y., Shi, J., Yang, L., Li, D., and Li, J.: Regional modeling of dust mass balance and radiative forcing over East Asia using WRF-Chem, Aeolian Research, 15, 15-30, http://dx.doi.org/10.1016/j.aeolia.2014.02.001, 2014.

Chen, S., Huang, J., Li, J., Jia, R., Jiang, N., Kang, L., Ma, X., and Xie, T.: Comparison of dust emissions, transport, and deposition between the Taklimakan Desert and Gobi Desert from 2007 to 2011. Science China Earth Sciences, 60(1), 1338-1355, doi:10.1007/s11430-016-9051-0, 2017.

Huang, J., Fu, Q., Su, J., Tang, Q., Minnis, P., Hu, Y., Yi, Y., and Zhao, Q.: Taklimakan dust aerosol radiative heating derived from CALIPSO observations using the Fu-Liou radiation model with CERES constraints, Atmos. Chem. Phys., 9, 4011-4021, doi:10.5194/acp-9-4011-2009, 2009.

Li, Z. Q., Xu, H., Li, K. T., Li, D. H., Xie, Y. S., Li, L., Zhang, Y., Gu, X. F., Zhao, W., Tian, Q. J., Deng, R. R., Su, X. L., Huang, B., Qiao, Y. L., Cui, W. Y., Hu, Y., Gong, C. L., Wang, Y. Q., Wang, X. F., Wang, J. P., Du, W. B., Pan, Z. Q., Li, Z. Z., and Bu, D.: Comprehensive Study of Optical, Physical, Chemical, and Radiative Properties of Total Columnar Atmospheric Aerosols over China: An Overview of Sun-Sky Radiometer Observation Network (SONET) Measurements, Bulletin of the American Meteorological Society, 99, 739-755, doi:10.1175/BAMS-D-17-0133.1, 2018.

Liu, L., Guo, J., Gong, H., Li, Z., Chen, W., Wu, R., Wang, L., Xu, H., Li, J., Chen, D., and Zhai, P.: Contrasting Influence of Gobi and Taklimakan Deserts on the Dust Aerosols in Western North America. Geophysical Research Letters, 46(15), 9064-9071, doi:10.1029/2019GL083508, 2019.

Liu, J., Zheng, Y., Li, Z., Flynn, C., Welton, E. J., and Cribb, M.: Transport, vertical structure and radiative properties of dust events in southeast China determined from ground and space sensors, Atmospheric Environment, 45(35), 6469-6480, doi:10.1016/j.atmosenv.2011.04.031, 2011b.

Liu, Z., Liu, D., Huang, J., Vaughan, M., Uno, I., Sugimoto, N., Kittaka, C., Trepte, C., Wang, Z., Hostetler, C., and Winker, D.: Airborne dust distributions over the Tibetan Plateau and surrounding areas derived from the first year of CALIPSO lidar observations, Atmos. Chem. Phys., 8, 5045–5060, doi:10.5194/acp-8-5045-2008, 2008.

Mikami, M., Shi, G., Uno, I., Yabuki, S., Iwasaka, Y., Yasui, M., Aoki, T., Tanaka, T.Y., Kurosaki, Y., Masuda, K., Uchiyama, A., Matsuki, A., Sakai, T., Takemi, T., Nakawo, M., Seino, N., Ishizuka, M., Satake, S., Fujita, K., Hara, Y., Kai, K., Kanayama, S., Hayashi, M., Du, M., Kanai, Y., Yamada, Y., Zhang, X.Y., Shen, Z., Zhou, H., Abe, O., Nagai, T., Tsutsumi, Y., Chiba, M., and Suzuki, J.: Aeolian dust experiment on climate impact: An overview of Japan-China joint project ADEC, Global and Planetary Change, 52, 142-172, doi:10.1016/j.gloplacha.2006.03.001, 2006.

Sun, H., Pan, Z., and Liu, X.: Numerical simulation of spatial-temporal distribution of dust aerosol and its direct radiative effects on East Asian climate, J. Geophys. Res., 117, doi:10.1029/2011JD017219, 2012.

Xia, X., and Zong, X.: Shortwave versus longwave direct radiative forcing by Taklimakan dust aerosols, Geophysical Research Letters, 36(7), L07803, doi:10.1029/2009GL037237, 2009.

Yuan, T., Chen, S., Huang, J., Wu, D., Lu, H., Zhang, G., Ma, X., Chen, Z., Luo, Y., and Ma, X.: Influence of Dynamic and Thermal Forcing on the Meridional Transport of Taklimakan Desert Dust in Spring and Summer. Journal of Climate, 32(3), 749-767, DOI: 10.1175/JCLI-D-18-0361.1, 2019.

Zhao, C., Liu, X., Leung, L. R., Johnson, B., Mcfarlane, S. A., Gustafson, W. I., Fast, J. D., and Easter, R. C.: The spatial distribution of mineral dust and its shortwave radiative forcing over North Africa: modeling sensitivities to dust emissions and aerosol size treatments, Atmos. Chem. Phys., 10, 8821-8838, doi:10.5194/acp-10-8821-2010, 2010.

2. Section 2 and 3, the authors seem to be drowned by abundant resources and avoid stringing them together to form a system. Some descriptions should be streamlined. The outline and structure of this manuscript should be reorganized.

Reply: Thank you also for pointing out these issues on the structure and the descriptions in Sections 2 and 3. We have made a number of changes in these respects.

First of all, as mentioned in the responds to the general comments, we restructured section 2 and rephrased the title of subsection 3.3.3 to make the structure more clear and compact: 1) subsection **"2.2 Aerosol properties during the DAO-K campaign" was moved out from this section**; 2) subsection **"2.1 Experimental site and instrumentation" was divided into "2.1 Observation site" and "2.2 Instrumentation"**; 3) subsection **"3.3.3 Experimental setup" was rephrased as "3.3.3 Model setup"** to avoid confuse with the subsection of "Instrumentation".

Secondly, we **modified the subsection "2.1 Observation site"** to explain why the experimental site was selected in Kashi instead of other main source region of Asian dust (e.g., Gobi Desert) and the representativeness of the experimental period to study the dust radiative forcing effects. Fig. 1 was also edited to focus on the location of experimental site.

Finally, we **reorganized Table 1 in subsection "2.2 Instrumentation" to summarize the parameters and instruments in three groups (i.e., applications in radiative transfer simulation, WRF-Chem simulation, as well as evidences and validation)**. The first two groups of parameters work as model inputs in section 3 (i.e., inputs of radiative transfer simulation and WRF-Chem model simulation, respectively). **Correspondingly, the introductions of experimental apparatus and data in this subsection were sorted into three groups and were arranged in three paragraphs**: 1) measurements of main data of aerosol properties (including sun-sky radiometer, continuous particulate monitor, and ambient air quality continuous automated monitoring system); 2) measurements of ancillary parameters of surface albedo and the vertical structure (including sounding balloons, OMI/Aura, MODIS/Terra+Aqua, pyrheliometer and pyranometers); 3) measurements of ancillary evidences of dust and cloud layers (including LILAS lidar and all sky view camera). The descriptions of each group contained data processing, quality control, and applications in this study. **Some detailed descriptions about the calibration of the sun-sky radiometers were removed to make the main line more concise.** Please find them the new subsection "2.2 Instrumentation" in the revised manuscript.

In these ways we hope to have tightened the structure and optimized the descriptions of the Section 2 and 3.

3. Section 2.1, this part should explain why the experimental site was selected in Kashi instead of the local aerosol properties, such as the representativeness or speciality in studying aerosol-related issues.

Reply: In response to the above comment (specific comment 2) we divided subsection"2.1 Experimental site and instrumentation" into two subsections "2.1 Observation site" and "2.2 Instrumentation" to make this part expressed in much cleaner, more structured manner. Following this comment, we have revised the subsection on experimental site so that the specialitis of aerosol property and aerosol radiation effect at Kashi site are more carefully introduced:

"**In addition to the Kashi station near the Taklimakan Desert, SONET also maintains two dust aerosol observation stations (i.e., Zhangye and Minqin stations) in the Gobi Desert which is another important source of Asian dust. Although some studies reported that the dust generated in Taklimakan Desert exerts a less influence on long-range downstream regions due to the unique terrain and low-level background wind climatology compared to those in Gobi Desert (Chen et al., 2017; Liu et al., 2019), Taklimakan Desert is more representative to study the effects of dust aerosol solar radiative forcing on local region than the Gobi Desert because of its huge dust emission capability (Chen et al., 2017).**"

"**According to the SONET long-term measurements from 2013, the Kashi site is frequently affected by dust, where the multi-year average *AOD* is up to 0.56±0.18 at 500 nm; moreover, the Ångström exponent (*AE*, 440~870 nm) and fine-mode fraction (*FMF*, 500 nm) at Kashi are the lowest (with the multi-year average values of 0.54±0.27 and 0.40±0.14, respectively) among all 16 sites within SONET around China (Li et al., 2018). In contrast, the multiyear average *AOD*s (500 nm) at Zhangye (0.28±0.11) and Minqin (0.26±0.11) are only half of that at Kashi or less (Li et al., 2018). Meanwhile, their average values of *AE* and *FMF* are also greater than those at Kashi (Li et al., 2018). They all imply coarse particles are more dominant in the Taklimakan Desert in comparison with the Gobi Desert.**"

Please find them in the subsection "2.1 Observation site" in the revised manuscript.

References:

Chen, S., Huang, J., Li, J., Jia, R., Jiang, N., Kang, L., Ma, X., and Xie, T.: Comparison of dust emissions, transport, and deposition between the Taklimakan Desert and Gobi Desert from 2007 to 2011. Science China Earth Sciences, 60(1), 1338-1355, doi:10.1007/s11430-016-9051-0, 2017.

Li, Z. Q., Xu, H., Li, K. T., Li, D. H., Xie, Y. S., Li, L., Zhang, Y., Gu, X. F., Zhao, W., Tian, Q. J., Deng, R. R., Su, X. L., Huang, B., Qiao, Y. L., Cui, W. Y., Hu, Y., Gong, C. L., Wang, Y. Q., Wang, X. F., Wang, J. P., Du, W. B., Pan, Z. Q., Li, Z. Z., and Bu, D.: Comprehensive Study of Optical, Physical, Chemical, and Radiative Properties of Total Columnar Atmospheric Aerosols over China: An Overview of Sun-Sky Radiometer Observation Network (SONET) Measurements, Bulletin of the American Meteorological Society, 99, 739-755, doi:10.1175/BAMS-D-17-0133.1, 2018.

Liu, L., Guo, J., Gong, H., Li, Z., Chen, W., Wu, R., Wang, L., Xu, H., Li, J., Chen, D., and Zhai, P.: Contrasting Influence of Gobi and Taklimakan Deserts on the Dust Aerosols in Western North America. Geophysical Research Letters, 46(15), 9064-9071, doi:10.1029/2019GL083508, 2019.

4. Lines 85-86, 'the Ångström exponent (AE, 440~870 nm) and fine-mode fraction (FMF) at Kashi are the lowest among all sites in China' What is the scientific value of this sentence? And it needs strong literature to support.

Reply: We changed this sentence into:

"**…moreover, the Ångström exponent (*AE*, 440~870 nm) and fine-mode fraction (*FMF*, 500 nm) at Kashi are the lowest (with the multi-year average values of 0.54±0.27 and 0.40±0.14, respectively) among all 16 sites within SONET around China (Li et al., 2018).**"

Please find it in the subsection "2.1 Observation site" in the revised manuscript. The scientific values of the multi-year average *AE* and *FMF* have been provided. The literature was also added.

References:

Li, Z. Q., Xu, H., Li, K. T., Li, D. H., Xie, Y. S., Li, L., Zhang, Y., Gu, X. F., Zhao, W., Tian, Q. J., Deng, R. R., Su, X. L., Huang, B., Qiao, Y. L., Cui, W. Y., Hu, Y., Gong, C. L., Wang, Y. Q., Wang, X. F., Wang, J. P., Du, W. B., Pan, Z. Q., Li, Z. Z., and Bu, D.: Comprehensive Study of Optical, Physical, Chemical, and Radiative Properties of Total Columnar Atmospheric Aerosols over China: An Overview of Sun-Sky Radiometer Observation Network (SONET) Measurements, Bulletin of the American Meteorological Society, 99, 739-755, doi:10.1175/BAMS-D-17-0133.1, 2018.

5. Section 2.2, 'aerosol properties during the DAO-K campaign' is part of the 'Results', so I suggest moving it to Section 4.

Reply: We agree with this point and have **moved the contents "aerosol properties during the DAO-K campaign" to section "4 Results of radiative transfer simulations"**. We realized that putting this part in section "2 Dust Aerosol Observation-Kashi field campaign" made the structure less understandable after the reviewer pointed it out. The reason being that in the previous manuscript these aerosol properties were input parameters for model simulations then were presented before the section "3 Estimation of aerosol solar radiation forcing". Following this

suggestion, we decided to include this part in the section of results (i.e., "4 Results of radiative transfer simulations"). We also reduced the descriptions on aerosol properties during the DAO-K campaign and focused on the aerosol properties relating to solar radiative forcing and efficiency. Please find them in the first paragraph in the subsection "4.1 Aerosol solar radiative forcing and efficiency".

6. The structure of the manuscript makes me feel that some parts are more or less irrelevant to the title 'Solar radiative forcing of aerosol particles near the Taklimakan desert during the Dust Aerosol Observation-Kashi campaign in Spring 2019'. Too much attention was spent on Section 4.3.

Reply: The improvements of dust radiative forcing estimation and the evaluation of the model results are the main points of this manuscript. We recognize that such improvement of solar radiative forcing estimation and the comprehensive evaluations of model results in the manuscript may provide meanings for dust radiative forcing research in different regions and also can be extended to other kind of aerosol particles. Besides structuring contents into a more understandable format (see the reply to the general comments), we changed the title into "**Aerosol solar radiative forcing near the Taklimakan Desert based on radiative transfer and regional meteorological simulations during the Dust Aerosol Observation-Kashi campaign**" to make the topic more clearly and completely to be expressed.

To avoid too much contents in section 4 and to highlight the comparison and evaluation of the radiative transfer and WRF-Chem simulations in the manuscript, **subsection "4.3 Comparisons and validation" was isolated from section 4 and changed to "5 Comparison with WRF-Chem simulations".** The old subsection "4.3.1 Comparison between radiative transfer simulations and AERONET results" was renamed as "4.3 Difference from AERONET products", and was moved to follow the section 4.2 to state and discuss the results of radiative transfer simulations together.

<u>Responses to technical comments:</u>

1. Line 17, 'are improved by' should be changed to 'were improved by'.

Reply: **Changed as suggested**. Please see line 17 in the revised manuscript.

2. Line 40, 'it is a challenging' should be changed to 'it is challenging' or 'it is a challenge'.

Reply: It has been **changed to "it is still challenging"**. Please see line 39 in the revised manuscript.

3. Line 41, add 'the' before 'high surface albedo over desert'.

Reply: **Added as suggested.** Please see line 40 in the revised manuscript.

4. Line 42, I suggested replacing the sentence 'Numerous efforts have investigated…' with 'Numerous efforts have been undertaken to investigate…'.

Reply: **Replaced as suggested.** Please see lines 34-35 in the revised manuscript.

5. Line 52, 'have relatively small inter-annual variation' should be changed to 'had relatively small inter-annual variation'.

Reply: **Changed as suggested.** Please see lines 101-102 in the revised manuscript.-

6. Line 53, 'According to WRF-Chem simulations' should be changed to 'According to the WRF-Chem simulations'.

Reply: **The sentence has been removed in the revised manuscript.**

7. Line 85, the comma before 'moreover' should be changed to semicolon.

Reply: **Changed as suggested.** Please see line 94 in the revised manuscript.

8. Line 239, 'includes' should be changed to 'included'.

Reply: **Changed as suggested.** Please see line 249 in the revised manuscript.

9. Line 315, 'Globally' should be changed to 'Generally'.

Reply: **Changed as suggested.** Please see line 345 in the revised manuscript.

10. Line 433, 'for it will damage the surface-layer particulate results' should be changed to 'for that it will damage the surface-layer particulate results'.

Reply: **Changed as suggested.** Please see lines 460-461 in the revised manuscript.

11. I suggest deleting some acronyms, especially the phrases only appear once. Too many acronyms make the article chaotic.

Reply: Some less common acronyms, like **“ TD” (Taklimakan Desert), “ LOA” (Laboratoire d'Optique Atmosphérique), “ CNEMS” (China National Environmental Monitoring Center), “BEC” (background error covariance), were deleted** in the revised manuscript.

To Anonymous Reviewer #2: (Comment ID:acp-2020-60-RC2)

Dear Reviewer,

Thank you very much for your detailed and supportive comments. You raised important issues in the comments. They can help us to improve the manuscript to a better scientific level. We have carefully taken these comments into consideration and have revised our manuscript accordingly. Please find below the comments in blue italics and our responses in black and the changes in bold.

Responses to major comments:

1. P2L35-38: This sentence is confusing to me. If my understanding is right, it is meant to express the dust originated from Taklimakan Desert (TD) exerts influences the air quality and climate over the downstream regions via long-range transport. Therefore, please try to be specific instead of using general words. However, some key references are missing, since both observations (Liu et al., 2019, doi:10.1029/2019GL083508.) and model simulations (Chen et al., 2017, doi: 10.1007/s11430-016-9051-0) suggested that the dusts generated in TD have LESS impacts on downstream regions due to the unique terrain and low-level background wind climatology, compared with those from other deserts in northwestern China.

Reply: We thank the reviewer for pointing out these issues around influences of dust aerosol particles originated from Taklimakan Desert. In response to the comments, we have rephrased this sentence in a more specific way. The suggested references have been added. Please find them in the second paragraph of section "1 Introduction" in the revised manuscript:

"**As one of the largest sandy deserts in the world, the Taklimakan Desert located in the Xinjiang Uygur Autonomous Region of China is a main source region of Asian dust (Huang et al., 2009), which influences not only surrounding areas such as the Tibetan Plateau (Liu et al., 2008; Chen et al., 2013; Yuan et al., 2019), but also wide regions in Eastern Asia (Mikami et al., 2006; Liu et al., 2011b; Yuan et al., 2019), even North America and Greenland through long-range transports across the Pacific Ocean (Bory et al., 2003; Chen et al., 2017; Liu et al., 2019).**"

The issue of less impacts of Taklimakan dust particles on downstream regions due to the unique terrain and low-level background wind climatology, and the reason that the experimental site was

selected near Taklimakan desert instead of the Gobi desert were also referred and discussed. Please find them in the subsection "2.1 Observation site" in the revised manuscript:

"**In addition to the Kashi station near the Taklimakan Desert, SONET also maintains two dust aerosol observation stations (i.e., Zhangye and Minqin stations) in the Gobi Desert which is another important source of Asian dust. Although some studies reported that the dust generated in Taklimakan Desert exerts a less influence on long-range downstream regions due to the unique terrain and low-level background wind climatology compared to those in Gobi Desert (Chen et al., 2017; Liu et al., 2019), Taklimakan Desert is more representative to study the effects of dust aerosol solar radiative forcing on local region than the Gobi Desert because of its huge dust emission capability (Chen et al., 2017).**"

"**According to the SONET long-term measurements from 2013, the Kashi site is frequently affected by dust, where the multi-year average *AOD* is up to 0.56±0.18 at 500 nm; moreover, the Ångström exponent (*AE*, 440~870 nm) and fine-mode fraction (*FMF*, 500 nm) at Kashi are the lowest (with the multi-year average values of 0.54±0.27 and 0.40±0.14, respectively) among all 16 sites within SONET around China (Li et al., 2018). In contrast, the multiyear average *AOD*s (500 nm) at Zhangye (0.28±0.11) and Minqin (0.26±0.11) are only half of that at Kashi or less (Li et al., 2018). Meanwhile, their average values of *AE* and *FMF* are also greater than those at Kashi (Li et al., 2018). They all imply coarse particles are more dominant in the Taklimakan Desert in comparison with the Gobi Desert.**"

References:

Bory, A. J., Biscaye, P. E., and Grousset, F. E.: Two distinct seasonal Asian source regions for mineral dust deposited in Greenland (NorthGRIP), Geophys. Res. Lett., 30, 1167, doi:10.1029/2002GL016446, 2003.

Chen, S., Huang, J., Zhao, C., Qian, Y., Leung, L. R., and Yang, B.: Modeling the transport and radiative forcing of Taklimakan dust over the Tibetan Plateau: A case study in the summer of 2006, J. Geophys. Res. Atmos., 118, 797-812, doi:10.1002/jgrd.50122, 2013.

Chen, S., Huang, J., Li, J., Jia, R., Jiang, N., Kang, L., Ma, X., and Xie, T.: Comparison of dust emissions, transport, and deposition between the Taklimakan Desert and Gobi Desert from 2007 to 2011. Science China Earth Sciences, 60(1), 1338-1355, doi:10.1007/s11430-016-9051-0, 2017.

Huang, J., Fu, Q., Su, J., Tang, Q., Minnis, P., Hu, Y., Yi, Y., and Zhao, Q.: Taklimakan dust aerosol radiative heating derived from CALIPSO observations using the Fu-Liou radiation model with CERES constraints, Atmos. Chem. Phys., 9, 4011-4021, doi:10.5194/acp-9-4011-2009, 2009.

Mikami, M., Shi, G., Uno, I., Yabuki, S., Iwasaka, Y., Yasui, M., Aoki, T., Tanaka, T.Y., Kurosaki, Y., Masuda, K., Uchiyama, A., Matsuki, A., Sakai, T., Takemi, T., Nakawo, M., Seino, N., Ishizuka, M., Satake, S., Fujita, K., Hara, Y., Kai, K., Kanayama, S., Hayashi, M., Du, M., Kanai, Y., Yamada, Y., Zhang, X.Y., Shen, Z., Zhou, H., Abe, O., Nagai, T., Tsutsumi, Y., Chiba, M., and Suzuki, J.: Aeolian dust experiment on climate impact: An overview of Japan-China joint project ADEC, Global and Planetary Change, 52, 142-172, doi:10.1016/j.gloplacha.2006.03.001, 2006.

Li, Z. Q., Xu, H., Li, K. T., Li, D. H., Xie, Y. S., Li, L., Zhang, Y., Gu, X. F., Zhao, W., Tian, Q. J., Deng, R. R., Su, X. L., Huang, B., Qiao, Y. L., Cui, W. Y., Hu, Y., Gong, C. L., Wang, Y. Q., Wang, X. F., Wang, J. P., Du, W. B., Pan, Z. Q., Li, Z. Z., and Bu, D.: Comprehensive Study of Optical, Physical, Chemical, and Radiative

Properties of Total Columnar Atmospheric Aerosols over China: An Overview of Sun-Sky Radiometer Observation Network (SONET) Measurements, Bulletin of the American Meteorological Society, 99, 739-755, doi:10.1175/BAMS-D-17-0133.1, 2018.

Liu, L., Guo, J., Gong, H., Li, Z., Chen, W., Wu, R., Wang, L., Xu, H., Li, J., Chen, D., and Zhai, P.: Contrasting Influence of Gobi and Taklimakan Deserts on the Dust Aerosols in Western North America. Geophysical Research Letters, 46(15), 9064-9071, doi:10.1029/2019GL083508, 2019.

Liu, J., Zheng, Y., Li, Z., Flynn, C., Welton, E. J., and Cribb, M.: Transport, vertical structure and radiative properties of dust events in southeast China determined from ground and space sensors, Atmospheric Environment, 45(35), 6469-6480, doi:10.1016/j.atmosenv.2011.04.031, 2011b.

Liu, Z., Liu, D., Huang, J., Vaughan, M., Uno, I., Sugimoto, N., Kittaka, C., Trepte, C., Wang, Z., Hostetler, C., and Winker, D.: Airborne dust distributions over the Tibetan Plateau and surrounding areas derived from the first year of CALIPSO lidar observations, Atmos. Chem. Phys., 8, 5045–5060, doi:10.5194/acp-8-5045-2008, 2008.

Yuan, T., Chen, S., Huang, J., Wu, D., Lu, H., Zhang, G., Ma, X., Chen, Z., Luo, Y., and Ma, X.: Influence of Dynamic and Thermal Forcing on the Meridional Transport of Taklimakan Desert Dust in Spring and Summer. Journal of Climate, 32(3), 749-767, DOI: 10.1175/JCLI-D-18-0361.1, 2019.

2. Figures 3, 5, 10, 12: The X-axis can be considered to be revised (more minor ticks and labels are needed to be given), given the ASRF and ASRFE are only able to be estimated during daytime without clouds. Another important issue is the cloud-induced impact on the radiation reaching the surface. The authors are better to analyze the day-by-day variation of cloud (fraction) over the study sites of Kashi, which is concurrent with the ground-based aerosol remote sensing and radiation observations. I believe this will provide more insights into the community of aerosol radiative forcing.

Reply: **More minor ticks and labels of the x-axes have been added in Figs. 4 (old Fig. 3), 5, 10**. For Fig. 12, in order to compare the WRF-Chem simulations and observations point by point, we interpolated the observations of $PM_{2.5}$, PM_{10}, and *AOD* at 675 nm to the corresponding assimilation time of 0:00, 6:00, 12:00 and 18:00 UTC of each day. Please also see the statement "The second one-month simulation was assimilated the observations of $PM_{2.5}$, PM_{10} and *AOD* with GSI at 0:00, 6:00, 12:00 and 18:00 UTC with the assimilation window of ±3 h centered at the analysis time." in the first paragraph of subsection "3.3.3 Model setup". So, the ticks and labels were given with daily intervals in Fig. 12. For each day, there are four sets of $PM_{2.5}$, PM_{10} in Figs. 12a and c. But normally less than four sets of *AOD* can be obtained owing to cloud screening or other quality control operation (see Fig. 12e). **To clarify this, the caption of Fig. 12 has been changed into: "Comparisons of the surface-layer $PM_{2.5}$ (a, b), PM_{10} (c, d) concentrations and *AOD* at 675 nm (e, f) among the observations, the WRF-Chem simulations with and without data assimilations (DA) in April 2019. The observations have been interpolated to 0:00, 6:00, 12:00, 18:00 UTC of each day."**

We thank the comment on cloud-induced impacts which raises an important issue. We fully agree with the reviewer that the magnitudes of direct solar radiative forcing of aerosol particles are affected by above, surrounding, and underlying clouds. The information of day-by-day variation of cloud fraction is valuable for estimation of solar radiation reaching the land surface. However, the cloud-induced impact on the radiation at surface is beyond the direct scope of this paper. "The focus of this study is to quantify of direct *ASRF* and *ASRFE* at the TOA, BOA, and in ATM under cloud-free sky conditions …" (see Paragraph 1 of the subsection "3.2 Radiative transfer simulation"). The cloud-free conditions were controlled by cloud screening and quality assurance procedures utilizing multi-angle observations of the sun-sky radiometer through the almucantar and principal plane scans in the entire sky before inversion (Smirnov et al., 2000; Holben et al., 2006; Li et al., 2015, 2018; Giles et al., 2019). The measurements of all sky view camera were also adopted as the ancillary evidences to assess cloud presence in this study. Inevitably, few small clouds out of the observation directions and super-thin clouds may escape from the cloud detection processing. They have impacts on the radiation reaching the surface more or less. However, to obtain the fraction of these clouds, the existing cloud detection methods should be significantly improved. We thank the reviewer for pushing us on this point and this issue will be considered in subsequent research.

References:

Giles, D. M., Sinyuk, A., Sorokin, M. S., Schafer J. S., Smirnov, A., Slutsker, I., Eck, T. F., Holben, B. N., Lewis, J. R., Campbell, J. R., Welton, E. J., Korkin, S. V., and Lyapustin, A. I.: Advancements in the Aerosol Robotic Network (AERONET) Version 3 database - Automated near-real-time quality control algorithm with improved cloud screening for Sun photometer aerosol optical depth (AOD) measurements, Atmospheric Measurement Techniques, 12, 169-209, doi:10.5194/amt-12-169-2019, 2019.

Holben, B. N., Eck, T. F., Slutsker, I., Smirnov, A., Sinyuk, A., Schafer, J., Giles, D., and Dubovik, O. : Aeronet's version 2.0 quality assurance criteria, Proceedings of SPIE - The International Society for Optical Engineering, 6408, doi: 10.1117/12.706524, 2006.

Li, Z., Li, D., Li, K., Xu, H., Cheng, X., Chen, C., Xie, Y., Li, L., Li, L., Li, W., Lv, Y., Qie, L., Zhang, Y., and Gu, X.: Sun/sky radiometer observation network with the extension of multi-wavelength polarization measurements, Journal of Remote Sensing, 19, 496-520, doi:10.11834/jrs.20144129, 2015.

Li, Z. Q., Xu, H., Li, K. T., Li, D. H., Xie, Y. S., Li, L., Zhang, Y., Gu, X. F., Zhao, W., Tian, Q. J., Deng, R. R., Su, X. L., Huang, B., Qiao, Y. L., Cui, W. Y., Hu, Y., Gong, C. L., Wang, Y. Q., Wang, X. F., Wang, J. P., Du, W. B., Pan, Z. Q., Li, Z. Z., and Bu, D.: Comprehensive Study of Optical, Physical, Chemical, and Radiative Properties of Total Columnar Atmospheric Aerosols over China: An Overview of Sun-Sky Radiometer Observation Network (SONET) Measurements, Bulletin of the American Meteorological Society, 99, 739-755, doi:10.1175/BAMS-D-17-0133.1, 2018.

Smirnov, A., Holben, B. N., Eck, T. F., Dubovik, O., and Slutsker, I.: Cloud-Screening and Quality Control Algorithms for the AERONET Database, Remote Sensing of Environment, 73(3), 337-349, doi:10.1016/S0034-4257(00)00109-7, 2000.

3. Figure 11: The readers would like to know how the ASRF is derived from AERONET, instead of the performance of ASRF product. The details will shed light on the difference between ASRF from RT model and ASRF from AERONET.

Reply: In response to this comment we have added more details about how the *ASRF* is derived from AERONET and the difference from the AERONET definition. Please find them in the first paragraph of subsection "4.3 Difference from AERONET products" in the revised manuscript:

"For AERONET, broadband upward and downward irradiances in the SW ranges from 0.2 to 4.0 μm were calculated by radiative transfer model with retrieved aerosol properties as model inputs (http://aeronet.gsfc.nasa.gov). However, AERONET adopts different definition of *ASRF* that only taking the downward irradiance at the BOA and the upward irradiance at the TOA into consideration (García et al., 2012). The upward irradiances with and without aerosols in Eq. (2), along with the downward irradiances with and without aerosols in Eq. (1), are not taken into account. Omitting the downward irradiances will not make much difference in *ASRF* at the TOA. But for *ASRF* at the BOA, it is predictable that neglecting the upward irradiance will lead to obvious difference."

References:

García, O. E., Díaz, J. P., Expósito, F. J., Díaz, A. M., Dubovik, O., Derimian, Y., Dubuisson, P., and Roger, J. C.: Shortwave radiative forcing and efficiency of key aerosol types using AERONET data, Atmos. Chem. Phys., 12, 5129-5145, doi:10.5194/acp-12-5129-2012, 2012.

Responses to minor comments:

1. Abstract: What are the two simulations in "The percent difference of daily mean ASRF between the two simulations." ? which is supposed to be described specifically.

Reply: Following this comment, we specified the two simulations in this sentence. It has been rewritten as "**The percent difference of daily mean *ASRF* between the RT and WRF-Chem simulations may exceed 50 % in heavy dust episode**". Please find it in lines 22-23 in the abstract of the revised manuscript.

2. P2L34: The dust aerosol originated from western China was revealed to exert significant impact on the mesoscale convection in downwind regions such as North China (Li et al., 2017,

doi: 10.1038/s41598-017-12681-0), which exemplified well the dynamic effect of dust. Therefore, this reference can be considered to be added here.

Reply: We thank the reviewer for the comment and providing reference. We have carefully review the literature. The suggested reference has been added:

"**Mineral dust is the most abundant large aerosol type in the atmosphere (Ansmann et al., 2011), which has a tremendous impact on radiation budget, not only through scattering process, but also due to absorption of solar (0.3~5 μm), also called shortwave (SW) radiation (Otto et al., 2007; García et al., 2012; Valenzuela et al., 2012; Lenoble et al., 2013), with potential dynamic consequences (Wendisch et al., 2008; Li et al., 2017).**"

Please find it in lines 31-34 of the section "1 Introduction" in the revised manuscript.

References:

Ansmann, A., Petzold, A., Kandler, K., Tegen, I., Wendisch, M., Müller, D., Weinzierl, B., Müller, T., and Heintzenberg, J.: Saharan Mineral Dust Experiments SAMUM-1 and SAMUM-2: What have we learned? Tellus, 63B, 403-429. doi:10.1111/j.1600-0889.2011.00555.x, 2011.

García, O. E., Díaz, J. P., Expósito, F. J., Díaz, A. M., Dubovik, O., Derimian, Y., Dubuisson, P., and Roger, J. C.: Shortwave radiative forcing and efficiency of key aerosol types using AERONET data, Atmos. Chem. Phys., 12, 5129-5145, doi:10.5194/acp-12-5129-2012, 2012.

Lenoble, J., Remer, L., and Tanré, D.: Aerosol Remote Sensing, Springer Berlin Heidelberg, doi:10.1007/978-3-642-17725-5, 2013.

Li, R., Dong, X., Guo, J., Fu, Y., Zhao, C., Wang, Y., and Min, Q.: The implications of dust ice nuclei effect on cloud top temperature in a complex mesoscale convective system, Sci Rep, 7, 13826, https://doi.org/10.1038/s41598-017-12681-0, 2017.

Otto, S., de Reus, M., Trautmann, T., Thomas, A., Wendisch, M., and Borrmann, S.: Atmospheric radiative effects of an in-situ measured Saharan dust plume and the role of large particles. Atmos. Chem. Phys., 7, 4887-4903, 2007.

Valenzuela, A., Olmo, F. J., Lyamani, H., Anton, M., Quirantes, A., and Alados-Arboledas, L.: Aerosol radiative forcing during African desert dust events (2005–2010) over Southeastern Spain, Atmos. Chem. Phys., 12, 10331-10351, doi:10.5194/acp-12-10331-2012, 2012.

Wendisch, M., Hellmuth, O., Ansmann, A., Heintzenberg, J., Engelmann, R., Althausen, D., Eichler, H., Müller, D., Hu, M., Zhang, Y., and Mao, J.: Radiative and dynamic effects of absorbing aerosol particles over the Pearl River Delta, China, Atmos. Environ., 42, 6405-6416, doi:10.1016/j.atmosenv.2008.02.033, 2008.

3. P2L34-35: Recent studies also show that the dust RF strongly depends on the overlapping pattern of dust aerosol and cloud layer in the vertical. Therefore, this sentence might as well be revised to "The dust radiative effects also depend on the surface albedo over the desert (Bierwirth et al., 2009) and the underlying clouds as well (Waquet et al., 2013, doi: 10.1002/2013GL057482; Xu et al., 2017, doi: 10.1016/j.atmosenv.2017.07.036)".

Reply: We thank the reviewer for pointing out this issue. We rephased this sentence as:

"**Moreover, the dust radiative effects also depend on the surface albedo over the desert and the cloud layer in the vertical as well (Bierwirth et al., 2009; Waquet et al., 2013; Xu et al., 2017).**"

Please find it in lines 40-41 of the section "1 Introduction" in the revised manuscript.

References:

Bierwirth, E., Wendisch, M., Ehrlich, A., Heese, B., Tesche, M., Althausen, D., Schladitz, A., Müller, D., Otto, S., Trautmann, T., Dinter, T., von Hoyningen-Huene, W., and Kahn, R.: Spectral surface albedo over Morocco and its impact on radiative forcing of Saharan dust, Tellus, 61B, 252-269, DOI: 10.1111/j.1600-0889.2008.00395.x, 2009.

Waquet, F., Peers, F., Ducos, F., Goloub, P., Platnick, S., Riedi, J., Tanré, D., and Thieuleux, F.: Global analysis of aerosol properties above clouds, Geophysical Research Letters, 40(21), 5809-5814, doi:10.1002/2013GL057482, 2013.

Xu, H., Guo, J., Wang, Y., Zhao, C., Zhang, Z., Min, M., Miao, Y., Liu, H., He, J., Zhou, S., and Zhai, P: Warming effect of dust aerosols modulated by overlapping clouds below, Atmospheric Environment, 166, 393-402, http://dx.doi.org/10.1016/j.atmosenv.2017.07.036, 2017.

4. P2L50: "were used" should be revised.

Reply: The sentence "For these estimates, simulations by the regional climate model version 4 (RegCM4) for the years of 2000~2009 were used" has been removed in the revised manuscript.

5.P2L58-61: what does "the modulate effects" mean? Besides, it seems strange in "performances of models…validated by comparing with the observations of AOD.." . I guess it is supposed to mean that ASRF from model …validated against that incorporating the observations of AOD…. Please clarify it or make modifications to them.

Reply: These sentences might be misleading. Here we were trying to say that comparisons of dust aerosol properties between the model simulations and the observations are not enough to confirm the dust radiative forcing simulations. The radiative forcing results estimated by various models should also be corroborated carefully against the direct observations of irradiances. We have revised these sentences to clarify this point:

"**The simulated results of dust aerosol radiative forcing have rarely been confirmed, especially in the Taklimakan Desert (Xia et al., 2009). Performances of various models sometimes were evaluated against the observations of aerosol optical depth (*AOD*), aerosol extinction profile, single scattering albedo (*SSA*), and particle size distribution (Zhao et al.,**

2010; Chen et al., 2014). Nevertheless, comparison of irradiance is indispensable to provide direct evidence for corroborating the *ASRF* simulated results."

Please find them in lines 55-60 in section "1 Introduction" in the revised manuscript.

References:

Chen, S., Zhao, C., Qian, Y., Leung, L. R., Huang, J., Huang, Z., Bi, J., Zhang, Y., Shi, J., Yang, L., Li, D., and Li, J.: Regional modeling of dust mass balance and radiative forcing over East Asia using WRF-Chem, Aeolian Research, 15, 15-30, http://dx.doi.org/10.1016/j.aeolia.2014.02.001, 2014.

Xia, X., and Zong, X.: Shortwave versus longwave direct radiative forcing by Taklimakan dust aerosols, Geophysical Research Letters, 36(7), L07803, doi:10.1029/2009GL037237, 2009.

Zhao, C., Liu, X., Leung, L. R., Johnson, B., Mcfarlane, S. A., Gustafson, W. I., Fast, J. D., and Easter, R. C.: The spatial distribution of mineral dust and its shortwave radiative forcing over North Africa: modeling sensitivities to dust emissions and aerosol size treatments, Atmos. Chem. Phys., 10, 8821-8838, doi:10.5194/acp-10-8821-2010, 2010.

6. P3L84: Please specify the years in "more than six years".

Reply: We specified the start year of the long-term observations at the Kashi site and rephrased this sentence to:

"**According to the SONET long-term measurements from 2013, the Kashi site is frequently affected by dust, where the multi-year average *AOD* is up to 0.56±0.18 at 500 nm;…**"

Please find it in lines 93-94 in subsection "2.1 Observation site" in the revised manuscript.

7. P3L85-85: it needs some references to support this statement "…the lowest among all sites in China. ". it really depends on the stations you refer to. e.g., the aerosol properties at Tazhong should be dominated by dust aerosol if you have observations therein.

Reply: We fully agree with this comment and rephrased this sentence to:

"…**moreover, the Ångström exponent (*AE*, 440~870 nm) and fine-mode fraction (*FMF*, 500 nm) at Kashi are the lowest (with the multi-year average values of 0.54±0.27 and 0.40±0.14, respectively) among all 16 sites within SONET around China (Li et al., 2018).**"

Please find it in lines 94-96 in the subsection "2.1 Observation site" in the revised manuscript.

References:

Li, Z. Q., Xu, H., Li, K. T., Li, D. H., Xie, Y. S., Li, L., Zhang, Y., Gu, X. F., Zhao, W., Tian, Q. J., Deng, R. R., Su, X. L., Huang, B., Qiao, Y. L., Cui, W. Y., Hu, Y., Gong, C. L., Wang, Y. Q., Wang, X. F., Wang, J. P., Du, W. B., Pan, Z. Q., Li, Z. Z., and Bu, D.: Comprehensive Study of Optical, Physical, Chemical, and Radiative Properties of Total Columnar Atmospheric Aerosols over China: An Overview of Sun-Sky Radiometer Observation Network (SONET) Measurements, Bulletin of the American Meteorological Society, 99, 739-755, doi:10.1175/BAMS-D-17-0133.1, 2018.

8. P5L122-123: More details are needed for the sounding measurements, including the launching time and location, sampling resolution, data uncertainties, e.t.c. Reference support is required.

Reply: We added more detailed descriptions of the sounding balloon measurements. The launching time and location were specified. Actually, the sampling resolutions of the measurements were not fixed. They always changed with the local atmospheric conditions at the balloon releasing time. Thus, we used the number of atmospheric layers in the vertical profile as well as the lowest and the highest layers in the atmosphere to sketch the sampling grids. They are valuable information to specify the vertical profiles in the radiative transfer model. Uncertainties in the sounding measurements of the whole pressure, temperature, and relative humidity profiles at Kashi station have not been reported in literatures. However, according to China Meteorological Administration, the measurement procedure was standardized and the data quality was guaranteed following the operational specifications for conventional upper-air meteorological observations. The corresponding reference support was provided. To address this comment, we added the descriptions about the sounding measurements as follow:

"**During the campaign, atmospheric profiles, including the vertical distributions of the atmospheric pressure, temperature, and relative humidity, were collected from sounding balloon measurements operated by Kashi regional meteorological bureau. Data quality was controlled following the operational specifications for conventional upper-air meteorological observations (China Meteorological Administration, 2010). The sounding balloons incorporate radiosondes were regularly launched twice a day around 0:00 and 12:00 UTC at Kashi weather station (39.46°N, 75.98°E, 1291 m above mean sea level). Normally there were more than 60 layers were specified from land surface to over 35 km.**"

Please find them in lines 130-136 in the subsection "2.2 Instrumentation".

References:

China Meteorological Administration, Operational specifications for conventional upper-air meteorological observations, China Meteorological Press, Beijing, China, 2010.

9. P7L149-151: I am confused again for the descriptions shown here are not consistent with those in Fig. 3. For instance, "The maximum PM10 concentration ..from 24 to 25 April 2019 was up

to 4 mg m-3" cannot be derived from Fig. 3. Also, "no CE318 measurement around the peak time of dust outbreak." disagreed with continuous AOD curves.

Reply: Here we were trying to explain that parts of the PM_{10} results were not shown in the original Fig. 3. Around the peak time of the heavy dust storm outbreak from 24 to 25 April 2019, the optical properties at some moments were not available due to the measurements of sun-sky radiometer in these conditions cannot satisfy the inversion criteria (Holben et al., 2006; Li et al., 2018). Thus, only the mass concentration results at the corresponding moments were presented for comparing with the CE318-derived aerosol optical depth and Ångström exponent parameters directly in this figure.

In the revised manuscript, we have tried to make the statements more concise and focused on descriptions of the aerosol properties relating to solar radiative forcing and efficiency. **Some less relevant and confusing details (e.g., "The maximum PM_{10} concentration during the heavy dust storm episode from 24 to 25 April 2019 was up to 4 mg m^{-3}. However, only moderate values of PM_{10} are shown in Fig. 3 because there was no CE318 measurement around the peak time of dust outbreak.") were removed from this context.** Following the suggestions from the other reviewer (specific comment 5 of "acp-2020-60-RC1"), this segment has been moved to the "Results" section. Please see the first paragraph of subsection "4.1 Aerosol solar radiative forcing and efficiency".

References:

Holben, B. N., Eck, T. F., Slutsker, I., Smirnov, A., Sinyuk, A., Schafer, J., Giles, D., and Dubovik, O. : Aeronet's version 2.0 quality assurance criteria, Proceedings of SPIE - The International Society for Optical Engineering, 6408, doi: 10.1117/12.706524, 2006.

Li, Z. Q., Xu, H., Li, K. T., Li, D. H., Xie, Y. S., Li, L., Zhang, Y., Gu, X. F., Zhao, W., Tian, Q. J., Deng, R. R., Su, X. L., Huang, B., Qiao, Y. L., Cui, W. Y., Hu, Y., Gong, C. L., Wang, Y. Q., Wang, X. F., Wang, J. P., Du, W. B., Pan, Z. Q., Li, Z. Z., and Bu, D.: Comprehensive Study of Optical, Physical, Chemical, and Radiative Properties of Total Columnar Atmospheric Aerosols over China: An Overview of Sun-Sky Radiometer Observation Network (SONET) Measurements, Bulletin of the American Meteorological Society, 99, 739-755, doi:10.1175/BAMS-D-17-0133.1, 2018.

List of all relevant changes made in the manuscript

(1) Section “1 introduction” was restructured to clarify the research background and significance, current status, concealed problems, as well as research mentality and content of this study.

(2) Old subsection “2.1 Experimental site and instrumentation” was divided into “2.1 Observation site” and “2.2 Instrumentation”.

we modified the subsection “2.1 Observation site” to explain why the experimental site was selected in Kashi instead of other main source region of Asian dust (e.g., Gobi Desert) and the representativeness of the experimental period to study the dust radiative forcing effects.

We also reorganized Table 1 in subsection “2.2 Instrumentation” to summarize the parameters and instruments in three groups (i.e., applications in radiative transfer simulation, WRF-Chem simulation, as well as evidences and validation). Correspondingly, the introductions of experimental apparatus and data in this subsection were sorted into three groups and were arranged in three paragraphs: 1) measurements of main data of aerosol properties; 2) measurements of ancillary parameters of surface albedo and the vertical structure; 3) measurements of ancillary evidences of dust and cloud layers. The descriptions of each group contained data processing, quality control, and applications in this study.

(3) Old subsection “2.2 Aerosol properties during the DAO-K campaign” was incorporated into subsection “ 4.1 Aerosol solar radiative forcing and efficiency”.

(4) subsection “3.3.3 Experimental setup” was rephrased as “3.3.3 Model setup” to avoid confuse with the subsection of “ Instrumentation”.

(5) Old section “4 Results and Discussion” was changed to “4 Results of radiative transfer simulations”.

(6) Old subsection “4.3 Comparisons and validation” was isolated from section 4 and changed to “5 Comparison with WRF-Chem simulations” to avoid too much contents in section 4.

(7) Subsection “4.3.1 Comparison between radiative transfer simulations and AERONET results” was renamed as “4.3 Difference from AERONET products”, and was moved to follow the section 4.2 to state and discuss the results of radiative transfer model simulations together.

Aerosol s~~S~~olar radiative forcing ~~of aerosol particles~~ near the Taklimakan D~~d~~esert based on radiative transfer and regional meteorological simulations during the Dust Aerosol Observation-Kashi campaign ~~in Spring 2019~~

Li Li[1], Zhengqiang Li[1], Wenyuan Chang[2], Yang Ou[1], Philippe Goloub[3], Chengzhe Li[4], Kaitao Li[1], Qiaoyun Hu[3], Jianping Wang[1], Manfred Wendisch[5]

[1]Aerospace Information Research Institute, Chinese Academy of Sciences, Beijing 100101, China
[2] Institute of Atmospheric Physics, Chinese Academy of Sciences, Beijing 100029, China
[3] Laboratoire d'Optique Atmosphérique, Université de Lille 1/CNRS, Lille 59655, France
[4] Department of Chemical and Biochemical Engineering, University of Iowa, Iowa 52242, USA
[5] Leipzig Institute for Meteorology, Leipzig University, Leipzig 04103, Germany

Correspondence to: Zhengqiang Li (lizq@radi.ac.cn)

Abstract. The Taklimakan D~~d~~esert is a main and continuous source of Asian dust particles causing a significant direct aerosol solar radiative forcing (*ASRF*). In order to improve the accuracy of the estimation of dust radiative forcing effects, the Dust Aerosol Observation-Kashi (DAO-K) campaign was carried out near the Taklimakan D~~d~~esert in April 2019. The objective of the campaign is to provide comprehensive parameters such as: dust optical and microphysical properties, vertical distribution and surface albedo, for the calculation of *ASRF*. The measurements were employed in radiative transfer (RT) simulations and the estimations were~~are~~ improved by considering the ~~actual~~ measured atmospheric profiles and diurnal variations of ~~land~~ surface albedo in addition to ~~reliable~~ aerosol parameters. The RT model estimates ~~the~~ daily averages of *ASRF* ~~results in average daily mean cooling effects~~ of -19 W m^{-2} at the top of atmosphere and -36 W m^{-2} at the bottom of atmosphere during the DAO-K campaign. The Weather Research and Forecasting model with Chemistry (WRF-Chem), with assimilations of measurements of the aerosol optical depth and particulate matter (*PM*) mass concentrations of particles with aerodynamic diameter smaller than 2.5 μm ($PM_{2.5}$) and 10 μm (PM_{10}),~~$PM_{2.5}$ and PM_{10} concentrations~~ measurements is prone to overestimate the radiative forcing effects of dust aerosols. The percent difference of daily mean *ASRF* between the RT and WRF-Chem~~two~~ simulations may exceed~~are greater than~~ 50 % in heavy dust episode. Ground-based observations of downward solar irradiances have confirmed~~validated~~ that the RT simulations are in good agreement with simultaneous observations, whereas the WRF-Chem estimations exhibit obvious discrepancy with the solar irradiance~~these independent~~ measurements. Data assimilations can partly reduce the discrepancy, but there is still room for improving the representation of dust aerosol radiative effects in the WRF-Chem simulations ~~of dust aerosol radiative forcing~~.

1 Introduction

Atmospheric aerosol particles play a vital role in regional and global climate changes, directly by modifying the radiation balance of the Earth-atmosphere system, and indirectly by altering cloud radiative properties, as well as cloud development and precipitation through acting as cloud condensation nuclei and/or ice nuclei (Twomey, 1977; IPCC, 2007; Lenoble et al., 2013; Werner et al., 2014). Mineral dust is the most abundant large aerosol type in the atmosphere (Ansmann et al., 2011), which has a tremendous impact on radiation budget, not only through scattering process, but also due to absorption of solar (0.3-5 μm), also called shortwave (SW) radiation (Otto et al., 2007; García et al., 2012; Lenoble et al., 2013), with potential dynamic consequences (Wendisch et al., 2008~~)~~; Li et al., 2017). Numerous efforts have been undertaken to investigate the SW radiative effects of mineral dust using radiative transfer (RT) model (e.g., Santa Barbara DISORT Atmospheric Radiative Transfer (SBDART), Fu-Liou RT model), or the regional and global meteorological and climate model (e.g., Weather Research and Forecasting model with Chemistry (WRF-Chem), Regional Climate Model version 4 (RegCM4)) by employing in-situ and remote sensing observations (Huang et al., 2009, 2014; Sun et al., 2012; Chen et al., 2013, 2014, 2018; Li et al., 2018). However, it is still challenging due to the high aerosol loading and complex light scattering properties of mineral dust. Moreover, t~~T~~he dust radiative effects also depend on the surface albedo over the desert and the cloud layer in the vertical as well (Bierwirth et al., 2009; Waquet et al., 2013; Xu et al., 2017).

As one of the largest sandy deserts in the world, the Taklimakan Desert ~~(TD)~~ located in the Xinjiang Uygh~~h~~ur Autonomous Region of China ~~(Fig. 1)~~ is a main source region of Asian dust (Huang et al., 2009), ~~which influences many areas in Eastern Asia, the Tibetan Plateau, the Pacific Ocean, even North America and Greenland (Bory et al., 2003; Mikami et al., 2006; Huang et al., 2009; Chen et al., 2013).~~ which influences not only surrounding areas such as the Tibetan Plateau (Liu et al., 2008; Chen et al., 2013; Yuan et al., 2019), but also wide regions in Eastern Asia (Mikami et al., 2006; Liu et al., 2011b; Yuan et al., 2019), even North America and Greenland through long-range transports across the Pacific Ocean (Bory et al., 2003; Chen et al., 2017; Liu et al., 2019). ~~Thus, a~~An accurate assessment of the Taklimakan aerosol solar radiative forcing (*ASRF*, defined as the difference of the net solar irradiance with and without aerosols presence) is important to evaluate regional and global climate changes. However, simulations by different models with different observation inputs varied widely in literatures. ~~However, it is a challenging due to the high aerosol loading and complex light scattering properties of mineral dust, as well as high surface albedo over desert. Numerous efforts have investigated the radiative effects of mineral dust over the Taklimakan region using radiative transfer (RT) model, or the regional and global meteorological and climate model (Huang et al., 2009, 2014; Sun et al., 2012; Chen et al., 2013, 2014, 2018).~~ Huang et al. (2009) employed the Fu-Liou RT model to simulate the Taklimakan *ASRF* during the dust episodes in the summer of 2006, and reported that the dust particles result in average daily mean SW warming of 14 W m^{-2} at the top of atmosphere (TOA), atmospheric warming of 79 W m^{-2}, and surface cooling of -65 W m^{-2}. ~~TD dust aerosols have a significant impact on solar radiation with the average daily mean radiative effects of 14 W m^{-2} at the top of atmosphere (TOA), 79 W m^{-2} in the atmosphere, and -65 W m^{-2} at the bottom of atmosphere (BOA).~~ Sun et al. (2012) adopted the RegCM4 simulations and ~~also~~ reported both negative *ASRF* (i.e., cooling effects) of dust particles at the

TOA and bottom of atmosphere (BOA) with the strongest values in spring during 2000~2009 period, reaching up to -4 W m^{-2} and -25 W m^{-2} in the Taklimakan Desert region, respectively. ~~negative *ASRF* of dust particles at BOA with the strongest values in spring, reaching up to -25 W m^{-2} in the three main desert regions of TD, western Inner Mongolia, and northern Xinjiang. For these estimates, simulations by the regional climate model version 4 (RegCM4) for the years of 2000~2009 were used. Chen et al. (2014) applied the Weather Research and Forecasting model with Chemistry (WRF-Chem) to investigate the seasonal and inter-annual variations of dust radiative forcing over TD during 2007~2011, and reported that the dust radiative forcing have relatively small inter-annual variation but a distinct seasonal course with maximum values in late spring and early summer. According to WRF-Chem simulations, the total (SW plus longwave) TD dust direct radiative forcing results in a TOA cooling of -5 W m^{-2}, atmospheric warming of up to 9 W m^{-2}, and BOA cooling of up to -14 W m^{-2} (Chen et al., 2014).~~ Li et al. (2018) also reported the negative ~~adopted the Santa Barbara (discrete ordinate radiative transfer) DISORT Atmospheric Radiative Transfer (SBDART) simulations to present the~~ multi-year average SW aerosol radiative forcing of -16 W m^{-2} at TOA and -18 W m^{-2} at BOA at the edge of ~~TD~~ Taklimakan Desert, Kashi station based on the SBDART simulations. The simulated results of dust aerosol radiative forcing have rarely been confirmed, especially in the Taklimakan Desert (Xia et al., 2009). ~~Large uncertainties in simulations of radiative forcing could cause significant errors in estimating the modulate effects of mineral dust aerosols on the climate (Huang et al., 2009). From previous researches, p~~Performances of various models ~~in simulating of dust *ASRF* have been~~ sometimes were ~~indirectly validated by comparing with~~ evaluated against the observations of aerosol optical depth (*AOD*), aerosol extinction profile, ~~aerosol~~ single scattering albedo (*SSA*), and particle size distribution (Zhao et al., 2010; Chen et al., 2014). Nevertheless, comparison of ~~*ASRF* or~~ irradiance is indispensable to provide direct evidence for ~~evaluating~~ corroborating the ~~models~~ *ASRF* simulated results.

An intensive dust field campaign is essential for comprehensive investigating the optical, physical, chemical, and radiative properties of dust aerosol particles over Taklimakan Desert. As such, one of the goals of the Dust Aerosol Observation-Kashi (DAO-K) field campaign is to provide high quality dataset on aerosol in this region to obtain accurate assessment of the Taklimakan aerosol solar radiative forcing. In this paper, we concentrate on estimation of direct solar radiative forcing of dust-dominated aerosols by the SBDART radiative transfer model with appropriate satellite and ground-based ~~observations as inputs~~ measurements of aerosol parameters, surface albedo, and atmospheric vertical profiles. The *ASRF* simulations will be comprehensively evaluated by comparison with the results of WRF-Chem simulations, ground-based irradiance measurements, as well as the AErosol RObotic NETwork (AERONET, http://aeronet.gsfc.nasa.gov) operational products (Holben et al., 1998).

The paper begins with a brief introduction of the ~~Dust-Aerosol-Observation-Kashi (~~DAO-K~~)~~ field campaign, and an ~~introduction~~ overview of the multi-source observations and data in Sect. 2. Methods ~~to~~for estimating ~~e~~ *ASRF* by improving the input ~~parameter~~s of atmospheric profiles and land surface albedo in RT simulation, and by employing data assimilations in the WRF-Chem simulation, are described in Sect. 3. Sect. 4 presents the ~~instantaneous and daily mean~~ results of *ASRF* simulated by RT model during the ~~DAO-K~~ field campaign and for some specific cases. The influences of the atmosphere and surface conditions on the results are discussed. ~~They are also evaluated by comparing with~~ The difference from the corresponding AERONET operational products~~,~~ are also analysed in this section. Direct comparison between the RT and WRF-Chem model

simulations~~,~~ is provided in Sect.5. ~~and~~ Both the model simulations are evaluated based on the simultaneous irradiance measurements. Summary and conclusions are given in Sect. ~~5~~6.

2 Dust Aerosol Observation-Kashi field campaign

2.1 Observation~~Experimental~~ site ~~and instrumentation~~

The Dust Aerosol Observation-Kashi ~~(DAO-K)~~ field campaign with comprehensive observations of physical, chemical, and optical properties of aerosol particles, radiative properties, vertical structures of atmosphere, and land surface albedo in ~~this~~ the Taklimakan Desert region was designed to provide high quality data for aerosol radiative forcing estimates. Kashi is located ~~in the vicinity of~~ at the edge of the Taklimakan Desert; it is surrounded by the Tianshan Mountains in the north, the Pamir Plateau in the west, and the Kunlun Mountains in the south (Fig. 1). The DAO-K field campaign was conducted at the Kashi campus of the Aerospace Information Research Institute, Chinese Academy of Sciences (39.50˚N, 75.93˚E, 1320 m above mean sea level). The campus hosts a long-term observation station within the Sun-sky radiometer Observation NETwork (SONET, www.sonet.ac.cn) (Li et al., 2018). In addition to the Kashi station near the Taklimakan Desert, SONET also maintains two dust aerosol observation stations (i.e., Zhangye and Minqin stations) in the Gobi Desert which is another important source of Asian dust. Although some studies reported that the dust generated in Taklimakan Desert exerts a less influence on long-range downstream regions due to the unique terrain and low-level background wind climatology compared to those in Gobi Desert (Chen et al., 2017; Liu et al., 2019), Taklimakan Desert is more representative to study the effects of dust aerosol solar radiative forcing on local region than the Gobi Desert because of its huge dust emission capability (Chen et al., 2017).

Kashi represents a typical place affected by dust aerosols, local anthropogenic pollution, and pollution transported from surrounding arid and desert areas. According to the SONET long-term measurements ~~during more than six years~~ from 2013, the Kashi site is frequently affected by dust ~~particles~~, where the multi-year average *AOD* is up to 0.56±0.18 at 500 nm~~,~~; moreover, the Ångström exponent (*AE*, 440~870 nm) and fine-mode fraction (*FMF*, 500 nm) at Kashi are the lowest (with the multi-year average values of 0.54±0.27 and 0.40±0.14, respectively) among all 16 sites ~~in~~within SONET around China (Li et al., 2018). In contrast, the multiyear average *AOD*s (500 nm) at Zhangye (0.28±0.11) and Minqin (0.26±0.11) are only half of that at Kashi or less (Li et al., 2018). Meanwhile, their average values of *AE* and *FMF* are also greater than those at Kashi (Li et al., 2018). They all imply coarse particles are more dominant in the Taklimakan Desert in comparison with the Gobi Desert. Every year, FMF reaches the lowest value, and the volume particle size distribution presents a pre-dominant coarse mode from March to May at Kashi (Li et al., 2018), due to the frequent dust invasions in spring ~~(Li et al., 2018)~~. Chen et al. (2014) also reported that the dust radiative forcing had relatively small inter-annual variation but a distinct seasonal course with the maximum values in late spring and early summer during 2007~2011 in the Taklimakan Desert. Sun et al. (2012) found that the SW radiative heating peaks appear in April in southern Xinjiang and in May for northern Xinjiang. Thus, the DAO-K intensive field campaign was carried out in April 2019 and lasted for nearly a month. During the campaign, several dust

processes were observed by coordinated deployment of multiple in-situ and remote sensing platforms and instruments based on passive and active detection technologies.

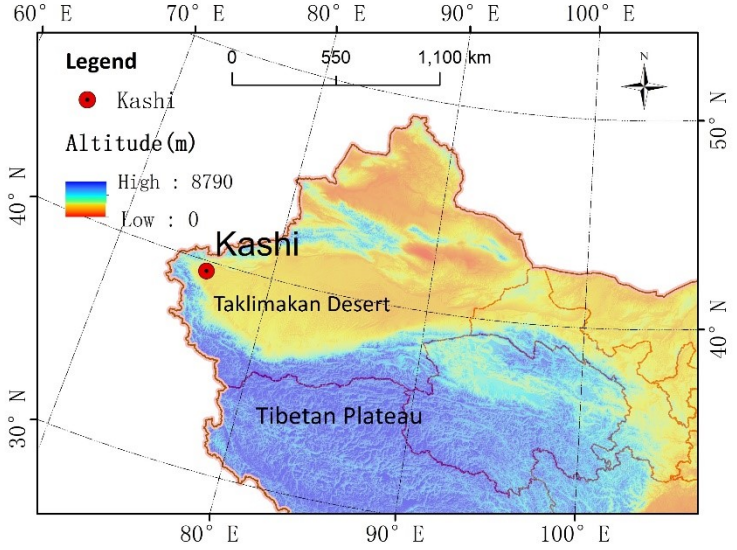

Figure 1: The location of the observation site (Kashi) during the DAO-K field campaign.

2.2 Instrumentation

Columnar aerosol properties are essential parameters for quantifying radiative forcing of atmospheric aerosol particles. However, high loading and complex light scattering process corresponding to diverse particle shapes bring challenges to remote sensing of mineral dust in the atmosphere (Dubovik et al., 2006; Bi et al., 2010; Li et al., 2019). Ground-based detection by sun-sky radiometer works out a solution by modelling dust particles as randomly oriented spheroids in the retrieval framework (Dubovik et al., 2006). ~~Fig. 2 shows the setup of the ground-based instrumentation in the DAO-K campaign, and Tab. 1 lists the corresponding ground-based and satellite-retrieved parameters applied in *ASRF* estimation and evaluation in this study.~~ Quality assured databases of aerosol properties are available based on both of AERONET and SONET sun-sky ratiometer retrievals (Holben et al. 1998; Li et al., 2018). During the DAO-K campaign, ~~F~~four Cimel sun-sky radiometers, including a polarized sun-sky-moon radiometer CE318-TP (#1150), two unpolarized sun-sky-moon radiometers CE318-T (#1098 and #1141), and a polarized sun-sky radiometer CE318-DP (#0971), were deployed at Kashi (Fig. 2a). CE318 #1150 and #1141were calibrated at AERONET Izaña Observatory by Langley plot approach with the accuracy of *AOD* about 0.25%~0.5% ~~at the visible and near-infrared bands and calibrated by integrating sphere with the uncertainty of radiance about 3%~5%~~ while *AOD*-related measurements and sky radiance measurements of CE318 #1098 and #0971 were calibrated via ~~inter-comparison with a~~ the master instrument #1150 ~~using Langley method and using~~by a vicarious/transfer calibration method before the field campaign~~, respectively (Li et al., 2008; 2018)~~ (Holben et al. 1998; Li et al., 2008, 2018). ~~to derive t~~The volume aerosol ~~properties~~ parameters of *AOD*, *SSA*, *AE*, ~~*SSA*,~~ and asymmetry factor (i.e., *g*) ~~for model inputs (Li et al., 2014, 2015)~~ in four channels with center wavelengths of 440, 675, 870, 1020 nm were retrieved following the SONET level 1.5 data

criteria (Li et al., 2018). ~~All the radiometers have been calibrated rigorously before the field campaign. The intensive measurements of four radiometers in this campaign aim to verify the consistencies of calibration coefficients. The volume aerosol parameters were combined with four radiometer measurements following SONET level 1.5 data criteria (Li et al., 2018).~~ Observations from the CE318~~-T~~ #1141 ~~during the DAO-K campaign~~ also joined in the AERONET dataset. The consistency of the products following the AERONET and SONET retrieval frameworks has been validated by Li et al. (2018). ~~In the retrieval frameworks, the dust particles were considered as non-spherical particles, which were modelled by randomly oriented spheroids (Dubovik et al., 2006).~~ The multi-wavelength properties of *AOD*, *SSA*, *AE*, and *g* were applied in radiative transfer model simulations. In addition to sun-sky radiometers, a METONE BAM-1020 Continuous Particulate Monitor was also deployed to measure $PM_{2.5}$ mass concentration (mg m^{-3}) (Fig. 2a). The hourly PM_{10} mass concentration (mg m^{-3}) were collected from the routine measurements of ambient air quality continuous automated monitoring system in Kashi operated by China National Environmental Monitoring Center. The aerosol parameters including *AOD*, $PM_{2.5}$ and PM_{10} mass concentrations were assimilated in WRF-Chem model simulation in this study.

Aerosol radiative effects also depend on the surface albedo and the vertical structure of atmosphere. During the campaign, atmospheric profiles, including the vertical distributions of the atmospheric pressure, temperature, and relative humidity, were collected from sounding balloon measurements operated by Kashi regional meteorological bureau. Data quality was controlled following the operational specifications for conventional upper-air meteorological observations (China Meteorological Administration, 2010). The sounding balloons incorporate radiosondes were regularly launched twice a day around 0:00 and 12:00 UTC at Kashi weather station (39.46˚N, 75.98˚E, 1291 m above mean sea level). Normally there were more than 60 layers were specified from land surface to over 35 km. In addition to pressure, temperature, and relative humidity profiles, ozone profiles obtained by the Ozone Monitoring Instrument (OMI)/Aura satellite (Bhartia et al., 1996) were also adopted as the RT model inputs. The satellite observations of Moderate resolution imaging spectroradiometer (MODIS)/Terra+Aqua were employed to collect the surface information during the DAO-K campaign. The MODIS products of shortwave bidirectional reflectance distribution function (BRDF) parameters, black-sky albedo (BSA), and white-sky albedo (WSA) were adopted to derive the surface albedo during the daytime (Schaaf and Wang, 2015). A solar radiation monitoring station, ~~consisting of~~equipped with an EKO MS-57 pyrheliometer and two MS-80 pyranometers, was used for measuring the direct, diffuse, and total solar irradiances (W m^{-2}) in the range of 280~3000 nm (Fig. 2a). The pyrheliometer and pyranometers have been calibrated before the campaign with uncertainties of 0.55% and 0.66%, respectively. They satisfy the requirements of class A under the ISO 9060:2018 with fast response time <0.2 s and <0.4 s, separately, which make them have excellent performances in understanding of the dynamics of solar irradiances in the atmosphere. The high-quality dataset of direct, diffuse, and total downward irradiances was applied in evaluation and validation of the RT and WRF-Chem simulations. The fraction of diffuse skylight radiation deduced from the diffuse and total irradiances also gave a key weighting index to modulate the diurnal-changes of the surface albedo.

Moreover, some other instruments provided independent evidences of the existences of dust and cloud layers in the atmosphere. Multiwavelength Mie-Raman polarization lidar (LILAS) developed by the Laboratoire d'Optique Atmosphérique,

~~(LOA) of University of Lille~~ Université de Lille 1(Fig. 2b), was equipped with three elastic wavelengths (all linearly polarized) at 355, 532, 1064 nm and three Raman wavelengths at 387, 530, 408 nm, from which the vertical distribution of multiple optical and physical properties of dust aerosol particles can be obtained (Veselovskii et al., 2016, 2018; Hu et al., 2019). The backscattering coefficient profile at 355 nm wavelength was applied in this study to distinguish the two-layer structure of dust. ~~$PM_{2.5}$ mass concentration was measured by a continuous particulate monitor. The hourly PM_{10} mass concentrations in Kashi were collected from the routine measurements operated by China National Environmental Monitoring Center (CNEMC).~~ The YNT all sky view camera ASC200 ~~cloud cover automatic observation instrument~~ equipped with two wide-dynamic full-sky visible and infrared imagers, ~~detected~~ recorded dynamic states of clouds ~~amount and distribution~~ in the whole sky during day and night with 10 min (or less than 10 min) resolution. ~~In addition to the ground-based observations, the satellite products of Moderate-resolution imaging spectroradiometer (MODIS)/Terra+Aqua were adopted to derive the diurnal change of the surface albedo (Schaaf and Wang, 2015). Ozone profiles obtained by the Ozone Monitoring Instrument (OMI)/Aura (Bhartia et al., 1996) were applied in the RT model input.~~ An overview of the instruments and corresponding parameters employed in the study is listed in Table 1. Considering different durations of various measurements, ~~in this study~~ we calculated and discussed the *ASRF* from 2 to 25 April 2019, when simultaneous measurements are available.

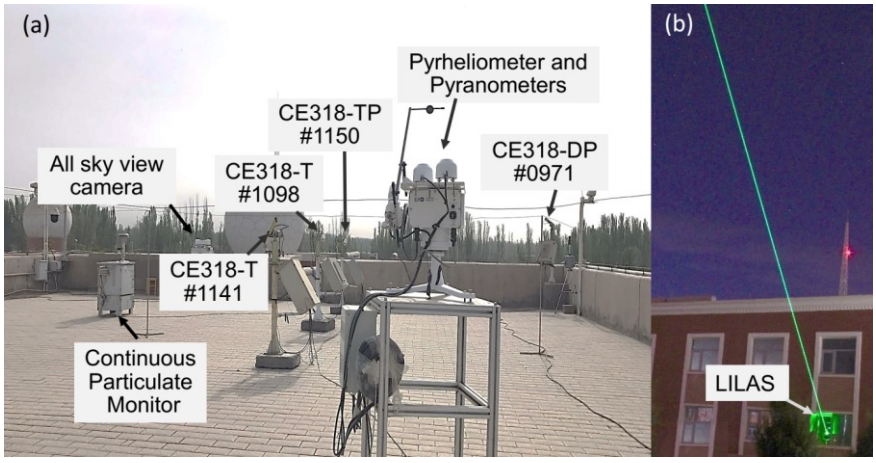

Figure 2: Setup of experimental apparatus ~~of~~during the DAO-K field campaign (a) on the roof, (b) in door.

Table 1: Overview of the p~~P~~arameters and instruments employed in the radiative transfer and WRF-Chem model simulations and validation. ~~used in this study from experimental and routine measurements during the DAO-K campaign.~~

Application	Parameter	Instrument	Duration
	aerosol properties		
	aerosol optical depth	sun-sky radiometer	1/4/2019~25/4/2019
Radiative transfer simulation	Ångström exponent		
	single scattering albedo		
	asymmetry factor		
	atmospheric profile		

	vertical distributions of atmospheric pressure, temperature, relative humidity	sounding balloon	1/4/2019~30/4/2019
	Ozone profile	OMI/Aura	1/4/2019~30/4/2019
	land surface albedo		
	shortwave BRDF parameters shortwave black-sky albedo shortwave white-sky albedo	MODIS/Terra+Aqua	1/4/2019~30/4/2019
	diffuse solar irradiance total solar irradiance	pyranometers	2/4/2019~28/4/2019
WRF-Chem simulation	aerosol optical depth	sun-sky radiometer	1/4/2019~25/4/2019
	$PM_{2.5}$ mass concentration	continuous particulate monitor	1/4/2019~28/4/2019
	PM_{10} mass concentration	ambient air quality continuous automated monitoring system	1/4/2019~30/4/2019
Evidences and validation	direct-normal solar irradiance diffuse solar irradiance total solar irradiance	pyrheliometer pyranometers	2/4/2019~28/4/2019
	backscattering coefficient	LILAS	4/4/2019~28/4/2019
	full-sky visible image	all sky view camera	2/4/2019~27/4/2019

~~Instrument~~	~~Parameter~~	~~Duration~~
~~Cimel sun-sky radiometer~~	~~aerosol optical depth (*AOD*)~~ ~~Ångström exponent (*AE*)~~ ~~single scattering albedo (*SSA*)~~ ~~asymmetry factor (*g*)~~	~~1/4/2019 – 25/4/2019~~
~~EKO MS-57 Pyrheliometer and MS-80 Pyranometers~~	~~direct-normal solar irradiance (W m^{-2})~~ ~~diffuse solar irradiance (W m^{-2})~~ ~~total solar irradiance (W m^{-2})~~	~~2/4/2019 – 28/4/2019~~

Multiwavelength Mie-Raman polarization lidar (LILAS)	backscattering coefficient ($km^{-1} sr^{-1}$)	4/4/2019 – 28/4/2019
ASC200 Cloud Cover Automatic Observation Instrument	full-sky visible image	2/4/2019 – 27/4/2019
METONE BAM-1020 Continuous Particulate Monitor	$PM_{2.5}$ mass concentration ($mg\ m^{-3}$)	1/4/2019 – 28/4/2019
Ambient air quality continuous automated monitoring system	PM_{10} mass concentration ($mg\ m^{-3}$)	1/4/2019 – 30/4/2019
Moderate resolution imaging spectroradiometer (MODIS)/Terra+Aqua	shortwave BRDF parameters shortwave black-sky albedo shortwave white-sky albedo	1/4/2019 – 30/4/2019
Sounding balloon	Vertical distributions of the atmospheric pressure, temperature, and relative humidity	1/4/2019 – 30/4/2019
Ozone Monitoring Instrument (OMI)/Aura	Ozone (O_3) profile	1/4/2019 – 30/4/2019

2.2 Aerosol properties during the DAO-K campaign

Fig. 3 illustrates the time series of *AOD*, *AE*, and corresponding $PM_{2.5}$ and PM_{10} mass concentrations measured during the DAO-K campaign. The average value of *AOD* at 550 nm is 0.65 during the campaign. According to *AOD*, five high aerosol loading episodes are identified: UTC 9:26~12:15 on 2/4/2019, 9:13 on 3/4/2019 until 5:11 on 5/4/2019, 1:52 on 8/4/2019 until 4:20 on 10/4/2019, 1:47 on 13/4/2019 until 12:32 on 16/4/2019, 1:30 on 24/4/2019 until 4:11 on 25/4/2019. The highest values of *AOD* at 550 nm (2.3) were observed from 24/4/2019 to 25/4/2019 during a severe dust storm event. There is an obvious negative correlation between *AOD* and *AE*. For these high aerosol loading episodes, the *AE*s show very low values, suggesting that the heavy aerosol outbreaks at Kashi were dominated by dust particles. As a qualitative indicator of aerosol particle size, the values of *AE* are always less than 1.0 during the DAO-K campaign, suggesting that aerosol particles around the Taklimakan desert are mainly dominated by coarse particles (even for clear situations). This is consistent with the results obtained in a previous study (Fig. 4 in Li et al., 2018). Comparatively high values of *AE* (>0.4) can be observed on 7, 12, 19, and 23 April 2019, implying enhanced local anthropogenic pollution and relatively small particle enrichments for these days.

The average values of $PM_{2.5}$ and PM_{10} mass concentrations corresponding to measuring times of CE318 are 0.08 and 0.25 $mg\ m^{-3}$ during the campaign, respectively. The time series of $PM_{2.5}$ and PM_{10} mass concentrations generally concur with that of *AOD*. However, for some days such as 19 and 23 April 2019, relatively high $PM_{2.5}$ corresponding to low *AOD* has been observed, also indicating the enhanced influences of anthropogenic pollutions in these cases. But for 7 and 12 April 2019, high

~~*AE* values corresponding to low $PM_{2.5}$ values could be down to the very low turbidity conditions. The errors in computations of *AE* significantly increase under low aerosol loading conditions (Kaskaoutis et al., 2007). The maximum PM_{10} concentration during the heavy dust storm episode from 24 to 25 April 2019 was up to 4 mg m^{-3}. However, only moderate values of PM_{10} are shown in Fig. 3 because there was no CE318 measurement around the peak time of dust outbreak.~~

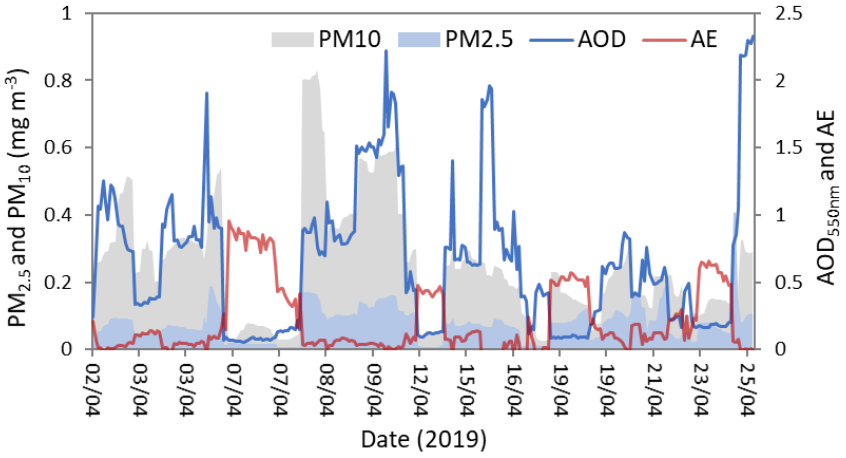

225

~~**Figure 3: Variations of aerosol optical depth (550 nm), Ångström exponent (440-870 nm), $PM_{2.5}$ and PM_{10} mass concentrations at Kashi site during the DAO-K campaign.**~~

3 Estimation of aerosol solar radiative forcing

3.1 Definition of aerosol solar radiative forcing

230 The direct solar radiative forcing of atmospheric aerosols can be calculated as (Babu et al.,2002; Adesina et al., 2014; Esteve et al., 2014):

$$ASRF_{\mathrm{TOA}} = F^{\mathrm{a}}_{\mathrm{net,TOA}} - F^{0}_{\mathrm{net,TOA}}, \quad (1)$$

$$ASRF_{\mathrm{BOA}} = F^{\mathrm{a}}_{\mathrm{net,BOA}} - F^{0}_{\mathrm{net,BOA}}, \quad (2)$$

$$ASRF_{\mathrm{ATM}} = ASRF_{\mathrm{TOA}} - ASRF_{\mathrm{BOA}}, \quad (3)$$

235 $$F_{\mathrm{net}} = F^{\downarrow} - F^{\uparrow}, \quad (4)$$

where $ASRF_{\mathrm{TOA}}$, $ASRF_{\mathrm{BOA}}$ and $ASRF_{\mathrm{ATM}}$ denote the direct aerosol solar radiative forcing at the TOA, BOA and in ATM, respectively. F^{a} and F^{0} indicate the net irradiances with and without aerosols, respectively. $F^{\downarrow}$ and $F^{\uparrow}$ separately represent the downward and upward irradiances. All the above quantities are in W m^{-2}. The radiative forcing efficiency is defined as the rate at which the atmosphere is forced per unit of aerosol optical depth at 550 nm (García et al., 2008, 2012):

$$ASRFE = ASRF / \tau_{550}, \quad (5)$$

where *ASRFE* (in W m^{-2} τ_{550}^{-1}) is the aerosol solar radiative forcing efficiency at the TOA, BOA, or in ATM. Since the effects of aerosol loading on radiative forcing have been eliminated, radiative forcing efficiency has unique advantage on evaluation of the direct radiative effects of different types of aerosols (García et al., 2008).

3.2 Radiative transfer ~~model~~ simulation

The focus of this study is to quantify of direct *ASRF* and *ASRFE* at the TOA, BOA, and in ATM under cloud-free sky conditions by the SBDART radiative transfer model with reliable satellite and ground-based observations during the DAO-K campaign as model inputs. SBDART is a radiative transfer software tool that has been widely applied~~dopted~~ in atmospheric radiative energy balance studies (Ricchiazzi et al.,1998; Li et al., 2018). The discrete ordinate method is adopted in the code, which provides a numerically stable algorithm to solve the equations of plane-parallel radiative transfer in a vertically inhomogeneous atmosphere (Ricchiazzi et al.,1998). The simulations cover the same wavelength range (i.e., 0.28~3.0 μm) with the pyranometer for ~~the~~ convenience of comparison. Simulations of the *ASRF* by RT model are susceptible to the input conditions including the aerosol properties, atmosphere profile ~~(including ozone)~~, and land surface albedo. They were specified based on the high-quality dataset obtained in the DAO-K campaign.

3.2.1 ~~Setting of a~~Aerosol properties

The aerosol properties including *AOD*, *SSA*, *AE*, and *g* were retrieved from the radiometer observations at four bands with the central wavelengths at 440, 675, 870, and 1020 nm. They were applied in the instantaneous radiative forcing and efficiency calculations at the corresponding observing time. The aerosol properties in the SW range are obtained by interpolation and extrapolation using parameters in the above mentioned four bands. For daily mean *ASRF* simulation, the averaged aerosol parameters (i.e., *AOD*, *SSA*, *AE*, and *g*) obtained from the day-time radiometer observations were used as alternatives of the daily mean aerosol properties. The daily mean aerosol radiative forcing and efficiency were calculated by taking the average of the 24 instantaneous values on an hourly basis.

3.2.2 ~~Setting of a~~Atmospheric profile

In addition to aerosol properties, atmospheric profiles of thermodynamic properties are important for *ASRF* calculation. The vertical distributions of air pressure, temperature, water vapor, and ozone densities have obvious influences on the direct and diffuse solar irradiances at the BOA. The predefined atmospheric profiles in RT model (e.g., tropical, mid-latitude summer, mid-latitude winter, sub-arctic summer, sub-arctic winter profiles) are different from Kashi local conditions. Within the *ASRF* simulations, the predefined profiles have been replaced by the actual measurements conducted during the campaign. Vertical distributions of the atmospheric pressure, temperature, relative humidity can be obtained by atmospheric sounding twice a day around 0:00 and 12:00 UTC at Kashi. The profiles of ozone density (in g m^{-3}) was deduced from the OMI/Aura OMO3PR

product (in DU) (Bhartia et al., 1996). Two atmospheric profiles were specified for each day. The profile closest to the *ASRF* simulated moment ~~of *ASRF*~~ was adopted for both of instantaneous and daily mean aerosol radiative forcing estimates.

3.2.3 ~~Setting of land s~~Surface albedo

Land surface albedo (LSA) is another key factor to influence the radiation budget, mainly due to its significant impact on the SW upward irradiance (Liang, 2004; Bierwirth et al., 2009; Tegen et al., 2009; Jäkel et al., 2013; Stapf et al., 2019). Land surface albedo α_{SW}, also known as blue-sky albedo, can be calculated from the black-sky albedo ~~(BSA)~~ $\alpha_{\mathrm{SW}}^{\mathrm{BSA}}$ and white-sky albedo ~~(WSA)~~ $\alpha_{\mathrm{SW}}^{\mathrm{WSA}}$ weighted by the fraction of diffuse skylight radiation (Schaaf et al., 2002; Wang et al., 2015):

$$\alpha_{\mathrm{SW}}(\theta_{\mathrm{s}},\varphi_{\mathrm{s}}) = f_{\mathrm{diffuse,SW}}\ \alpha_{\mathrm{SW}}^{\mathrm{WSA}} + (1-f_{\mathrm{diffuse,SW}})\ \alpha_{\mathrm{SW}}^{\mathrm{BSA}}(\theta_{\mathrm{s}},\varphi_{\mathrm{s}}), \tag{6}$$

where $f_{\mathrm{diffuse,SW}}$ denotes the fraction of diffuse radiation in the solar spectral range. $(\theta_{\mathrm{s}},\varphi_{\mathrm{s}})$ specifies the incident solar geometry (i.e., solar zenith angle and solar azimuthal angle).

The shortwave WSA and BSA are provided by the MODIS BRDF/Albedo Science Data Product MCD43A3, which is produced daily using 16 days of MODIS/Terra+Aqua data. MCD43A3 only delivers the surface albedo products at local solar noon. However, diurnal variations of LSA cannot be ignored, which has been demonstrated by several previous studies (Lewis and Barnsley, 1994; Lucht et al., 2000; Wang et al., 2015). There will be an obvious bias in estimating daily solar radiation when simply using the local noon value as a surrogate of daily mean albedo (Wang et al., 2015). As for the weighting parameters of the RossThickLiSparseReciprocal BRDF model (i.e., isotropic, volumetric, and geometric), the changes within 16 days are subtle. Therefore, the daily three model weighting parameters over the SW band afforded by the MODIS product MCD43A1 are adopted to derived the WSA and BSA (the latter is as a function of incident solar direction) at different *ASRF* simulated moments ~~of *ASRF*~~. The fraction of diffuse radiation can be calculated by the ratio of diffuse solar irradiance to total solar irradiance, which mainly depends on the solar zenith angle, aerosol and cloud conditions. The diffuse and total irradiances measured by pyranometers with 1 min resolution are applied in this study to calculate the fraction of diffuse radiation.

Fig. 34 gives diurnal variations of LSA and corresponding full-sky visible images under four typical sky conditions at Kashi. For the cloud-free clear sky ~~conditions~~ (almost the whole day of 7/4/2019 and afternoon of 12/4/2019), LSA changes distinctively for different time. High values of LSA can be observed in the early morning and the late afternoon. Meanwhile, the extreme value of LSA in the morning (0.253) is greater than that in the afternoon (0.218), which has been supported by some other field observations (Minnis et al., 1997; Wang et al., 2015). The local noon albedo shows very low value. The daily mean albedo under the clear-sky condition (0.199) is appreciably greater than the local noon albedo (0.173). In the dust-polluted (almost the whole days of 9/4/2019 and 25/4/2019) and cloudy (the morning of 12/4/2019) sky conditions, the changes of LSA are not as severely as in the clear-sky conditions. Nevertheless, the local noon albedo still cannot reflect the effects of aerosol and cloud variations on land surface albedo. Thus, diurnal-changed LSA and the daily mean albedo were adopted in

the instantaneous and daily mean *ASRF* simulations, respectively. It is predictable that estimations of instantaneous and daily mean aerosol radiative forcing can be improved by considering diurnal variations of LSA instead of local noon albedo.

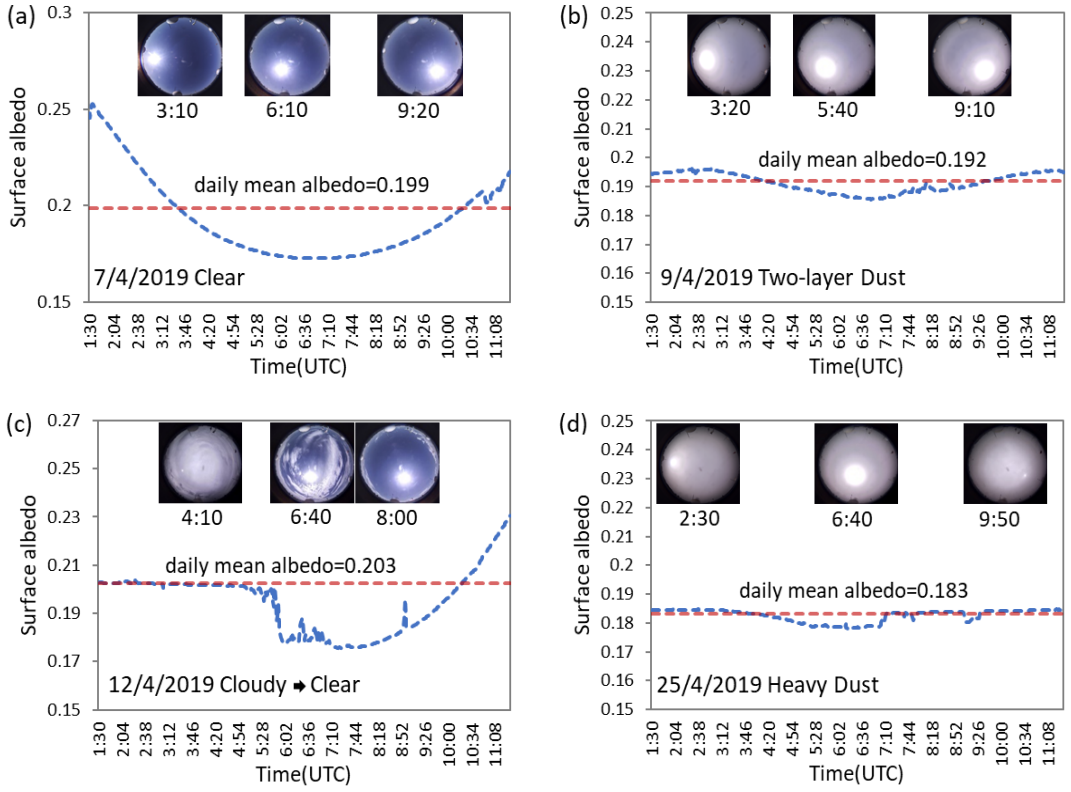

Figure 34: Diurnal variations of blue-sky albedo and corresponding full-sky visible images under different sky conditions at Kashi (a) clear case, (b) two-layer dust case, (c) clouds early/clearing late case, (d) heavy dust case.

3.3 WRF-Chem ~~model~~ simulation

3.3.1 Forecast model

The Weather Research and Forecasting model with chemistry (WRF-Chem) model version 4.0 (Grell et al., 2005; Fast et al., 2006) was also used to simulate the *ASRF* at Kashi. The simulations were configured in a 9 km domain centered at Kashi site with 45×45 grid points and 41 vertical levels that extended from the surface to 50 hPa. The main physical options used for this study included the Purdue Lin microphysics scheme, the unified Noah land surface model, the Yonsei University (YSU) scheme for planetary boundary layer meteorological conditions, and the Rapid Radiative Transfer Model for General Circulation Models (RRTMG) for SW and longwave radiation. The Carbon Bond Mechanism (CBMZ) was used for the Gas-phase chemistry processes (Zaveri and Peters, 1999), which include~~d~~s aqueous-phase chemistry. The aerosol chemistry was based on the Model for Simulating Aerosol Interactions and Chemistry (MOSAIC; Zaveri et al., 2008) with four size bins (0.039~0.156 μm, 0.156~0.625 μm, 0.625~2.5 μm, 5.0~10.0 μm dry diameters). The sum of aerosol mass concentrations in

315 the first three size bins constructs the concentration of $PM_{2.5}$ and the sum of the four size bins gives the concentration of PM_{10}. Aerosol types such as sulfate, methanesulfonate, nitrate, ammonium, black carbon, primary organic carbon, sodium, calcium, chloride, carbonate, aerosol liquid water, and other inorganic matter (e.g., trace metals and silica) are involved in the simulation. Dust was simulated with the GOCART dust emission scheme (Ginoux et al., 2001). The dust particulates were aggregated into the other inorganic matter component and were presented in the calculation of aerosol optical properties with anthropogenic
320 aerosols.

Aerosol optical properties were calculated as a function of wavelength based on the Mie theory. The aerosol components within each size bin are assumed to be internally mixed. The mixing refractive indexes are the volume-weight average in refractive indexes of all aerosol components. Aerosol extinction and scattering coefficients and asymmetry~~ic~~ factors for a particulate per size bin are attained though searching a look-up Mie table by Chebyshev polynomial interpolation with the
325 desired mixing refractive indexes and wet particulate radius. The value of particulate extinction coefficient multiplied with the particulate number concentration is volume extinction coefficient which is then multiplied with the height of layer to attain the layer *AOD* value. The sum of all layer *AOD* values over the four size bins is the columnar total *AOD* and is used for calculating *AOD* increments in the assimilation.

3.3.2 Assimilation system

330 Gridpoint Statistical Interpolation (GSI) 3DVAR assimilation system (Wu et al., 2002; Kleist et al., 2009) version 3.7 was applied to improve the simulated aerosols by assimilating the aerosol measurements at Kashi. This GSI version has been modified to assimilate the aerosol products (Liu et al., 2011; Schwartz et al., 2012). We assimilated our ground-based multi-wavelength AOD (440, 675, 870, 1020 nm) and the surface-layer concentrations of $PM_{2.5}$ and PM_{10} suited to the MOSAIC aerosol module in WRF-Chem. We used the natural logarithm of particulate number concentration per size bin as control
335 variables. The aerosol dry mass concentrations, particulate number concentrations and aerosol water contents are converted into *AOD* per size bin using the WRF-Chem aerosol optical routine. The adjoint observation operators for *AOD* and particulate matter are given as

$$\frac{\delta \ln(\tau)}{\delta \ln(n_i)} = \frac{n_i}{\tau} \cdot \frac{\delta \tau}{\delta n_i} = \frac{c_i}{\tau} \cdot e_i = \frac{\tau_i}{\tau}, \tag{7}$$

$$\frac{\delta \ln(c)}{\delta \ln(n_i)} = \frac{n_i}{c} \cdot \frac{\delta c}{\delta n_i} = \frac{n_i}{c} \cdot r_i, \tag{8}$$

340 where n_i is aerosol number concentration in the ith size bin, τ and c are the observed *AOD* and particulate matter mass concentrations. As no aerosol extinction coefficient assimilated in this experiment, we assume the extinction coefficient per size bin is constant in grid at each model layer. Innovation of number concentration due to *AOD* constraint is therefore a proportion of change in model layer *AOD* to the observed columnar *AOD*, which is attained via iteration to minimize the cost function. Innovation of number concentration due to the constraints of $PM_{2.5}$ and PM_{10} are associated with the ratios (r_i) of

mass concentrations to number concentrations in a size bin estimated in the guess field, weighted by the proportion of the size number concentration, changing in the iteration, to the total particulate matter concentration.

3.3.3 Model setup~~Experimental setup~~

Initial and lateral boundary conditions for the meteorological fields in the WRF-Chem simulations were generated from the National Centers for Environmental Prediction (NCEP) Final Analysis (FNL) data using the Global Forecast System (GFS) model at a horizontal resolution of 1°. The boundary conditions were updated every 6 h and then interpolated linearly in time by WRF-Chem. Anthropogenic emissions from the 2010 MIX emission inventories (www.meicmodel.org) containing the Multiresolution Emission Inventory of China (MEIC) were used in the simulations. The biogenic emissions were estimated using the Model of Emissions of Gases and Aerosols from Nature (MEGAN; Guenther et al., 2006). Two one-month WRF-Chem simulations were performed for April 2019, discarding a one-week spin-up at the beginning of each simulation. The first one-month simulation was used for modelling background error covariance ~~(BEC)~~. The second one-month simulation was assimilated the observations of $PM_{2.5}$, PM_{10} and *AOD* with GSI at 0:00, 6:00, 12:00 and 18:00 UTC with the assimilation window of ±3 h centered at the analysis times. The model was restarted from the meteorology and chemistry at analysis time and ran to the next analysis time. For the second one, each restart called the radiation routines twice which included and excluded the aerosols, respectively, and the corresponding difference between the two calls in irradiances is aerosol radiative forcing.

A general way to model background error covariance~~BEC~~ is the National Meteorological Center (NMC) method that computes the statistical differences between two forecasts with different leading lengths (e.g. 12 and 24 h, or 24 and 48 h) but valid at the same time (Parrish and Derber, 1992). However, in our experiment, the WRF-Chem model strongly underestimated aerosol concentrations and hence likely lowered the error magnitudes. For this reason, we assessed the standard deviations of the control variables over the entire one-month period at the four analysis hours (i.e., 0:00, 6:00, 12:00 and 18:00 UTC ~~00, 06, 12, 18 h~~), respectively. Each standard deviation field was used for modelling a background error covariance~~BEC~~ repeatedly applied in the assimilations at the corresponding analysis hour. This approach represents the strong fluctuations of control variables as weather evolution during clear and dusty days. We expect fluctuations of aerosols over the different weathers are larger than the uncertainties due to different leading forecast lengths and may give a better input field for modelling background error covariance~~BEC~~. The observation errors for *AOD* and *PM* were 50% of natural logarithm of 0.01 and those errors of *PM* including measurement error and representative error depending on the grid size and the *PM* concentrations (Schwartz et al., 2012). The choice of 50 % was determined by trying experimentally with different values, which can effectively assimilate measurements and will not excessively damage the model results.

4 Results ~~and Discussion~~of radiative transfer simulations

4.1 Aerosol solar radiative forcing and efficiency

~~Fig. 3 illustrates the time series~~The results of *AOD*, *AE*, ~~and corresponding~~ $PM_{2.5}$ and PM_{10} mass concentrations measured corresponding to CE318 observation time series during the DAO-K campaign are shown in Fig. 4. The average value of *AOD* at 550 nm is 0.65 during the campaign. According to *AOD*, five high aerosol loading episodes can be~~are~~ identified: UTC 9:26~12:15 on 2/4/2019, 9:13 on 3/4/2019 until 5:11 on 5/4/2019, 1:52 on 8/4/2019 until 4:20 on 10/4/2019, 1:47 on 13/4/2019 until 12:32 on 16/4/2019, 1:30 on 24/4/2019 until 4:11 on 25/4/2019. The highest values of *AOD* at 550 nm (2.3) were observed from 24/4/2019 to 25/4/2019 during a severe dust storm event. From Fig. 4, t~~T~~here is an obvious negative correlation between *AOD* and *AE*. For these high aerosol loading episodes, the *AE*s show very low values, suggesting that the heavy aerosol outbreaks at Kashi were dominated by dust particles. As a qualitative indicator of aerosol particle size, the values of *AE* are always less than 1.0 during the DAO-K campaign, indicating~~suggesting~~ that aerosol particles around the Taklimakan D~~d~~esert are mainly dominated by coarse particles (even for clear situations). This is consistent with the results obtained in a previous study (Fig. 4 in Li et al., 2018). Comparatively high values of *AE* (>0.4) can be observed on 7, 12, 19, and 23 April 2019, implying enhanced local anthropogenic pollution and relatively small particle enrichments for these days. ~~The average values of $PM_{2.5}$ and PM_{10} mass concentrations corresponding to measuring times of CE318 are 0.08 and 0.25 mg m^{-3} during the campaign, respectively.~~ The time series of $PM_{2.5}$ and PM_{10} mass concentrations generally concur with that of *AOD*. However, for some days such as 19 and 23 April 2019, relatively high $PM_{2.5}$ corresponding to low *AOD* has been observed, also indicating the enhanced influences of anthropogenic pollutions in these cases. But for 7 and 12 April 2019, high *AE* values corresponding to low $PM_{2.5}$ values could be down to the very low turbidity conditions. It should be noted that t~~T~~he errors in computations of *AE* significantly increase under low aerosol loading conditions (Kaskaoutis et al., 2007). ~~The maximum PM_{10} concentration during the heavy dust storm episode from 24 to 25 April 2019 was up to 4 mg m^{-3}. However, only moderate values of PM_{10} are shown in Fig. 3 because there was no CE318 measurement around the peak time of dust outbreak.~~

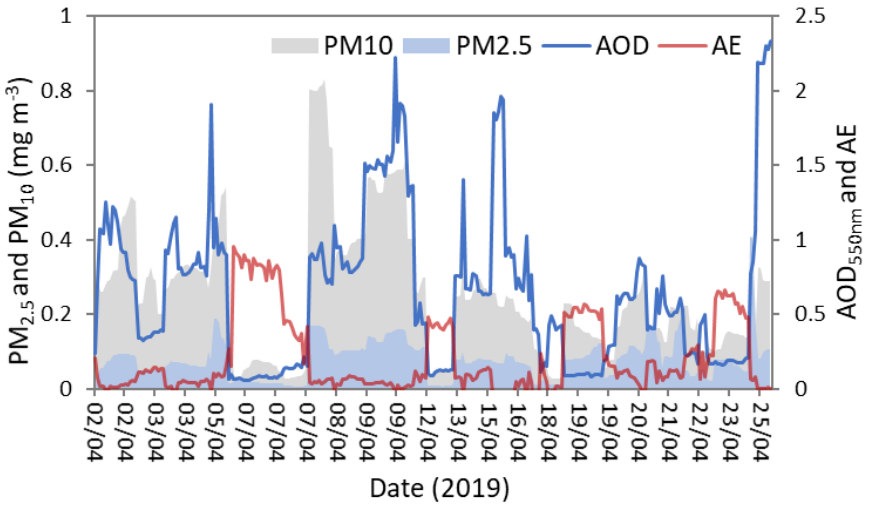

Figure ~~3~~4: Variations of aerosol optical depth (550 nm), Ångström exponent (440-870 nm), $PM_{2.5}$ and PM_{10} mass concentrations at Kashi site during the DAO-K campaign.

Results of instantaneous *ASRF* and *ASRFE* ~~at TOA, in ATM, at BOA~~ during the DAO-K campaign are given in Fig. 5. Both positive and negative values of *ASRF*, corresponding to warming and cooling effects respectively, can be found at top of the atmosphere (Fig. 5a). However, aerosols have only warming effects in the atmosphere (Fig. 5c) and cooling effects at the surface (Fig. 5e) during the DAO-K campaign. *ASRF*s at the TOA and BOA exhibit obvious negative correlations with *AOD*. But positive correlation can be observed between *ASRF* in the atmosphere and *AOD*. From Fig. 5, it is evident that the dust aerosol has strong influences on the solar radiation budget. For the five above ~~afore~~mentioned high aerosol loading episodes ~~(see Sect. 2.2)~~, the dust-dominant aerosols have stronger cooling effects at the TOA and BOA, and more significant warming effects in the atmosphere than other low aerosol loading situations. Moreover, the cooling effects at the BOA are more noticeable than which at the TOA, with the lowest values of -217 W m^{-2} and -119 W m^{-2}, respectively.

When *ASRF* is normalized by aerosol optical depth at 550 nm, the result of *ASRFE* is not sensitive to the aerosol loading. However, a weak negative correlation between *ASRFE* and *AE* can also be observed at the BOA (Fig. 5f). That means, the *ASRFE* at the surface can roughly indicate the radiative forcing effects of different types of aerosols (García et al., 2008). Relatively large fraction of small particles associated with high~~large~~ *AE* has stronger *ASRFE* for cooling the surface than other low *AE* situations. But for TOA and ATM (Fig. 5b, d), there ~~are~~is no obvious correlations between *ASRFE* and AE. ~~Globally~~ Generally, the cooling effect of aerosols at Kashi is more efficient at the BOA than that at the TOA. It~~That~~ is in accordance with the results of *ASRF*. In comparison with *ASRF*, the variation of *ASRFE* is relatively moderate during the campaign. The strongest cooling effects on the TOA and BOA all appear in the episode of dust storm outbreak (i.e., 24 and 25 April 2019) (see Fig. 5a, e). But large dust particles in this case do not show extreme radiative forcing efficiency (Fig. 5b, f). Strong cooling efficiencies at the surface during the DAO-K campaign occur in the very clear cases with high *AE* on 7 April 2019 (Fig. 5f).

During the DAO-K campaign, the average values of daily mean *ASRF* at Kashi are -19±13 W m^{-2} at the TOA and -36±23 W m^{-2} at the BOA, which are slightly stronger than the multiyear average values at this site (i.e., -16 W m^{-2} at the TOA and -

18 W m^{-2} at the BOA) obtained by the previous study (Li et al., 2018). These results are reasonable, since the campaign was performed in the dust-prone season and higher aerosol loading situations have stronger *ASRF* effects as discussed above. Likewise, the average values of daily mean *ASRFE* at the TOA and BOA during the DAO-K campaign are -27±9 W m^{-2} τ_{550}^{-1} and -55±10 W m^{-2} τ_{550}^{-1}, respectively, which are more efficient than the corresponding multiyear average values (i.e., -21 W m^{-2} τ_{550}^{-1} at the TOA and -24 W m^{-2} τ_{550}^{-1} at the BOA) reported in the previous study (Li et al., 2018).

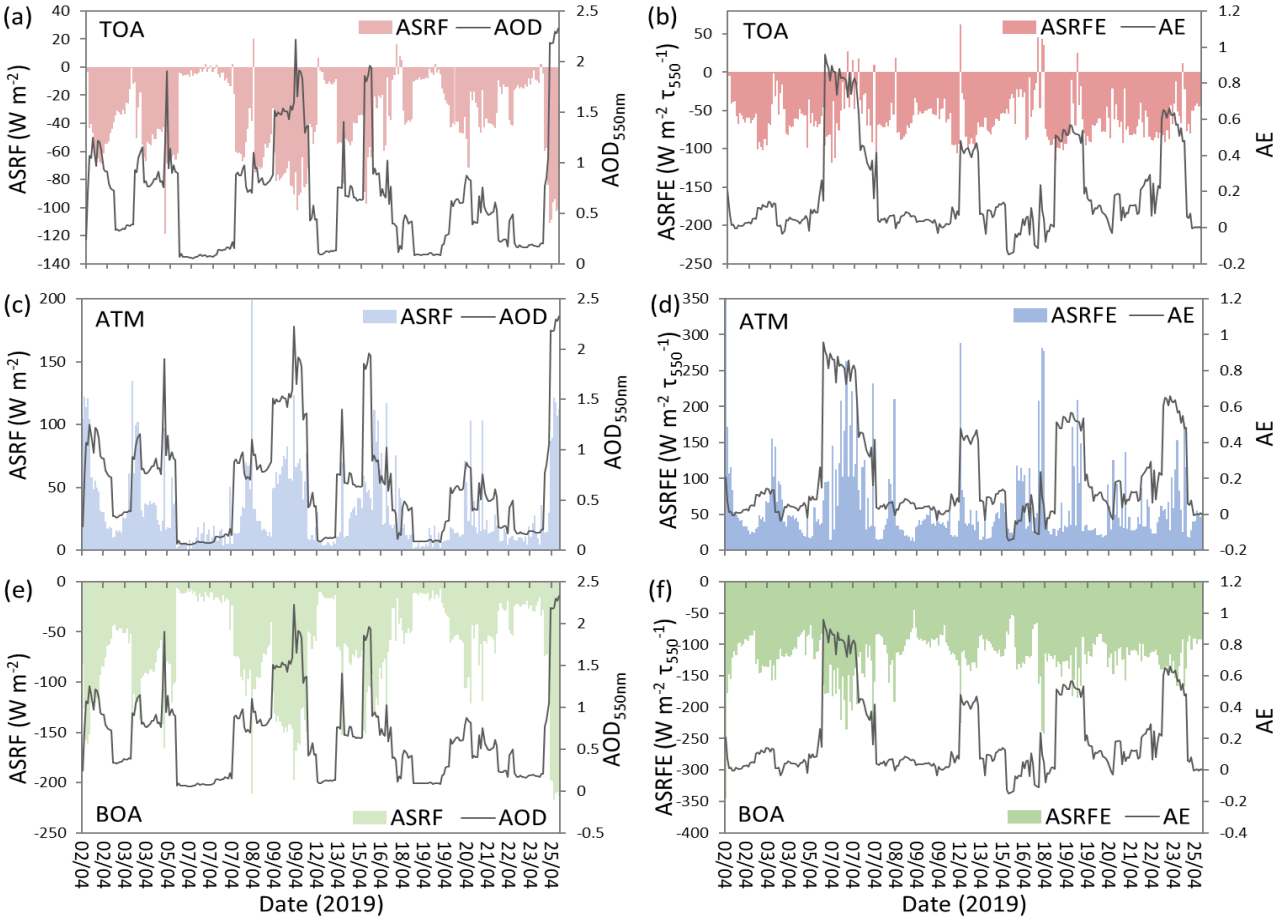

Figure 5: Instantaneous aerosol solar radiative forcing (left column) and efficiencies (right column) at Kashi site during the DAO-K campaign (upper panels: TOA; middle panels: ATM; lower panels: BOA).

4.1.1 Clear-sky case

Instantaneous *ASRF* and *ASRFE* of the clear sky case on 7 April 2019 is depicted in Fig. 6. It was a typical cloud-free day at Kashi with *AOD* at 550 nm less than 0.22 for the whole day. As discussed above, the highest *AE* is observed on this day during the one-month campaign (see Fig. 4~~3~~). Both cooling and warming effects of aerosols can be found at the top of atmosphere. The cooling effects of *ASRF* are up to -19 W m^{-2} at the TOA and -48 W m^{-2} at the BOA, and the warming effect of *ASRF* is

up to 50 W m^{-2} in the atmosphere. The corresponding extreme *ASRFE* values are -126, -236, and 263 W m^{-2} τ_{550}^{-1}, respectively

435 It is apparent that the changes of *ASRFE* are more intense than the corresponding *ASRF* for the clear case.

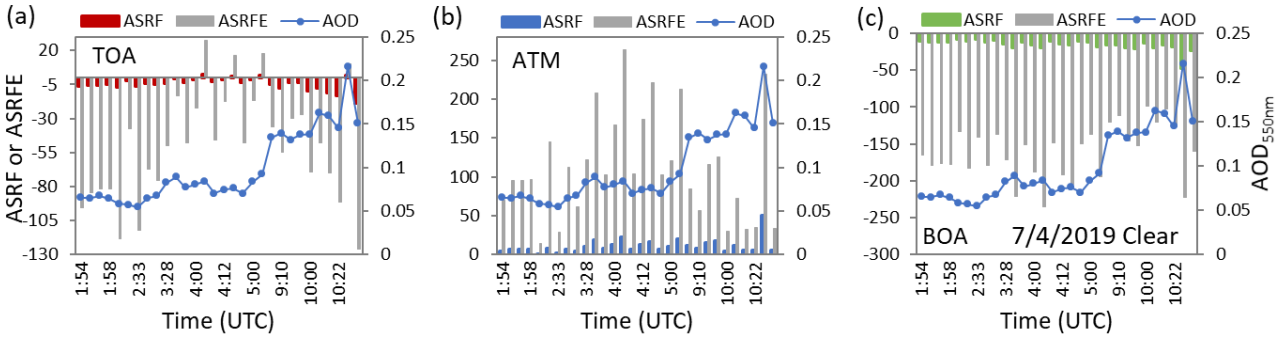

Figure 6: Instantaneous aerosol solar radiative forcing and efficiencies of the clear sky case on 7 April 2019 at Kashi site (a) TOA, (b) ATM, (c) BOA.

4.1.2 Heavy dust case

440 Fig. 7 describes *ASRF* and *ASRFE* for a heavy dust storm episode on 25 April 2019 at Kashi. Only few observations from 3:33 to 4:11 UTC were suitable for retrieval in this day. Aerosol optical depth at 550 nm was up to 2.3 during this observation period. In comparison with the clear case, dust particles have stronger cooling effects at the TOA and BOA (*ASRF*s up to -111 and -217 W m^{-2}, respectively), and stronger warming effect in ATM (*ASRF* up to 121 W m^{-2}). However, we observe the extreme *ASRFE* values of -51, -99, and 55 W m^{-2} τ_{550}^{-1} at the TOA, BOA, and in ATM, respectively, indicating that the radiative

445 forcing of dust is less efficient than that of the clear case. Moreover, the variations of *ASRFE* in the dust case are more moderate than which of *ASRF*. These are strikingly differen~~t~~ces from the clear-sky case.

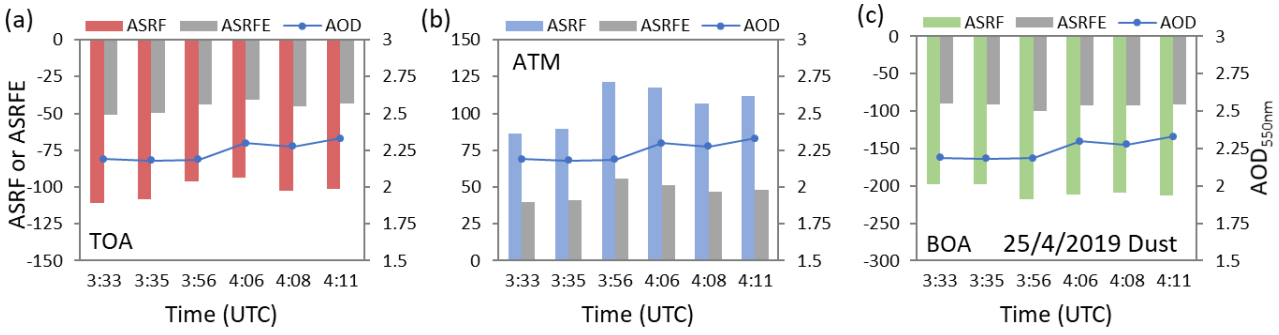

Figure 7: As Fig. 6, but for the heavy dust case on 25 April 2019.

4.1.3 Two-layer dust case

On 9 April 2019 one extra layer suspending above the planetary boundary layer (PBL) was observed. Fig. 8 illustrates the observations of LILAS on 8 April. Lidar observations on 9 April 2019 are not shown because the lidar stopped working due to technical problems in the night of 8 April 2019. According to the backscattering coefficient profiles at 355 nm, the lower layer and upper layer can be clearly identified. Lidar measurements indicate that aerosols in the layer above the PBL are probably dust particles because the derived high depolarization ratios agree with the values for dust. However, from lidar measurements we cannot draw unambiguous conclusion about the aerosol type in the PBL, because the incomplete overlap range of the lidar system is up to 800-1000 m. From Fig. ~~3~~4, high *AOD* corresponding to low *AE* in the whole atmosphere and high $PM_{2.5}$ and PM_{10} concentrations in the surface layer are exhibited from 8 to 9 April. It also suggests the complex pollutions by two-layer dust particles during this pollution process. *AOD* at 550 nm on 9 April changes from 1.4 to 2.2 (Fig. 9). In consistent with the above heavy dust case, only cooling effects can be observed at the TOA and BOA, and only warming effect can be found in ATM for this case. The two layers of dust particles result in a TOA cooling up to -102 W m^{-2}, BOA cooling of up to -198 W m^{-2}, and atmosphere warming of up to 123 W m^{-2}. The absolute values of *ASRF* at the TOA and BOA in this case are all less than those in the heavy dust case, suggesting the aerosols in the heavy dust case have more powerful ~~radiative forcing~~cooling effects. Nevertheless, the extreme values of *ASRFE* are -62, -105, and 58 W m^{-2} τ_{550}^{-1} at the TOA, BOA and in ATM, respectively, indicating that dust particles ~~have similar radiative forcing efficiencies in the two-layer and heavy dust cases.~~ in the two-layer case have stronger radiative forcing efficiencies than those in the heavy dust cases.

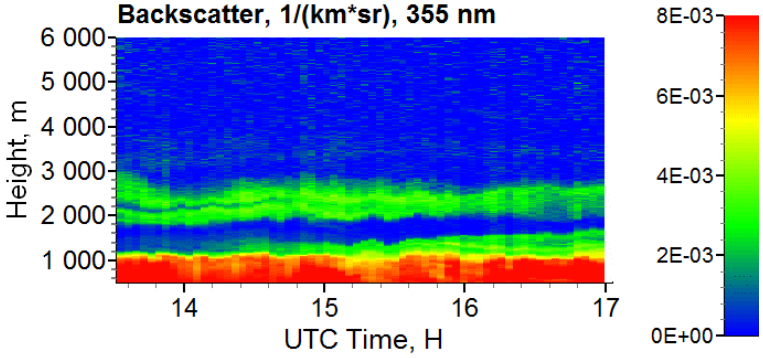

Figure 8: The backscattering coefficient profiles at 355 nm for the two-layer dust case in the night of 8 April 2019.

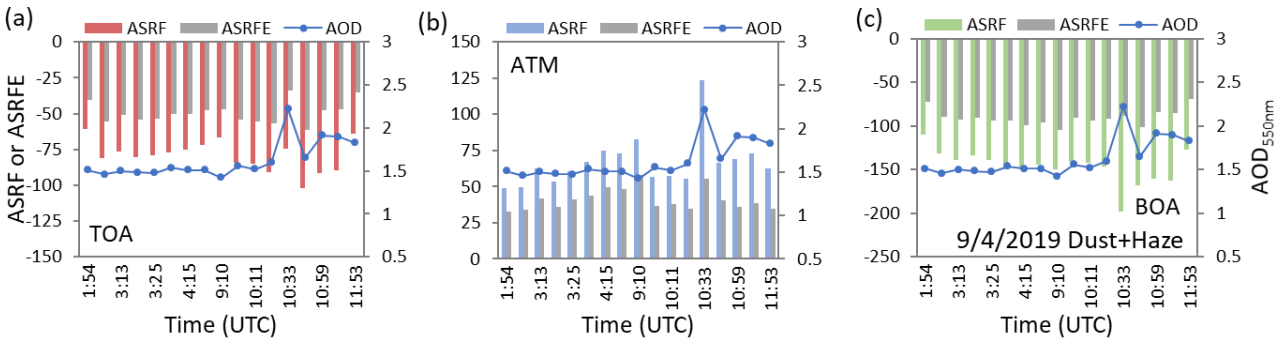

Figure 9: As Fig. 6, but for the two-layer dust case on 9 April 2019.

4.2 Influences of the atmosphere and surface conditions

Fig. 10 describes the influences of atmospheric profile and land surface albedo on the simulations of total irradiances and *ASRF*. The differences in the results of total downward irradiance (*TDI*), total upward irradiance (*TUI*), and *ASRF* at the TOA and BOA simulated with the pre-defined midlatitude winter profile and user-specified profiles, and simulated with local noon surface albedo and instantaneous surface albedo are given, respectively. According to Fig. 10a, different settings of profiles have no influence on the *TDI* at the TOA. For the *TUI*, the absolute differences are less than 9 W m^{-2}. However, the atmospheric profile has significant impacts on both the *TDI* and *TUI* at the surface. The influences on *TDI* are generally stronger than which on *TUI*. The maximum absolute difference is up to 138 W m^{-2} (Fig. 10c). For *ASRF* at the TOA, the effects of atmospheric profiles are less than 5 W m^{-2}. But the serious influences can up to 103 W m^{-2} on *ASRF* at the BOA (Fig. 10e). The average effect of different profiles on *ASRF* is 0.8 W m^{-2} at the TOA, which is quite small in comparison with the average values of daily *ASRF* (-19 W m^{-2}). However, the average difference of 13 W m^{-2} for *ASRF* affected by atmospheric profiles cannot be ignored relative to the average *ASRF* (-36 W m^{-2}) at the BOA. As a result, the cooling effects of aerosol radiative forcing will be significantly underestimated at the BOA simulated with the pre-defined midlatitude winter profile instead of the user-specified Kashi atmospheric profiles.

Like atmospheric profile, different settings of LSA have also no influence on *TDI* at the TOA (Fig. 10b). They have small effects on *TDI* at the BOA (absolute difference less than 3 W m^{-2}), but obvious impacts on *TUI* at the TOA and BOA (absolute difference up to 22 W m^{-2}) (Fig. 10 b,d). From Fig. 34, the local noon albedo is often less than the daily mean albedo. Especially for the clear day, the minimum of LAS occurs around the local noon. Then the *TUI* at the TOA and BOA will generally be underestimated by using the local noon albedo instead of instantaneous surface albedo in the simulations. But for *ASRF* (Fig. 10f), two LAS settings lead to moderate impacts at the TOA and BOA with average absolute differences of 1.8 and 1.7 W m^{-2}, respectively. Therefore, simulations using the local noon albedo trend to overestimate the cooling effects of the aerosol radiative forcing both at the TOA and BOA.

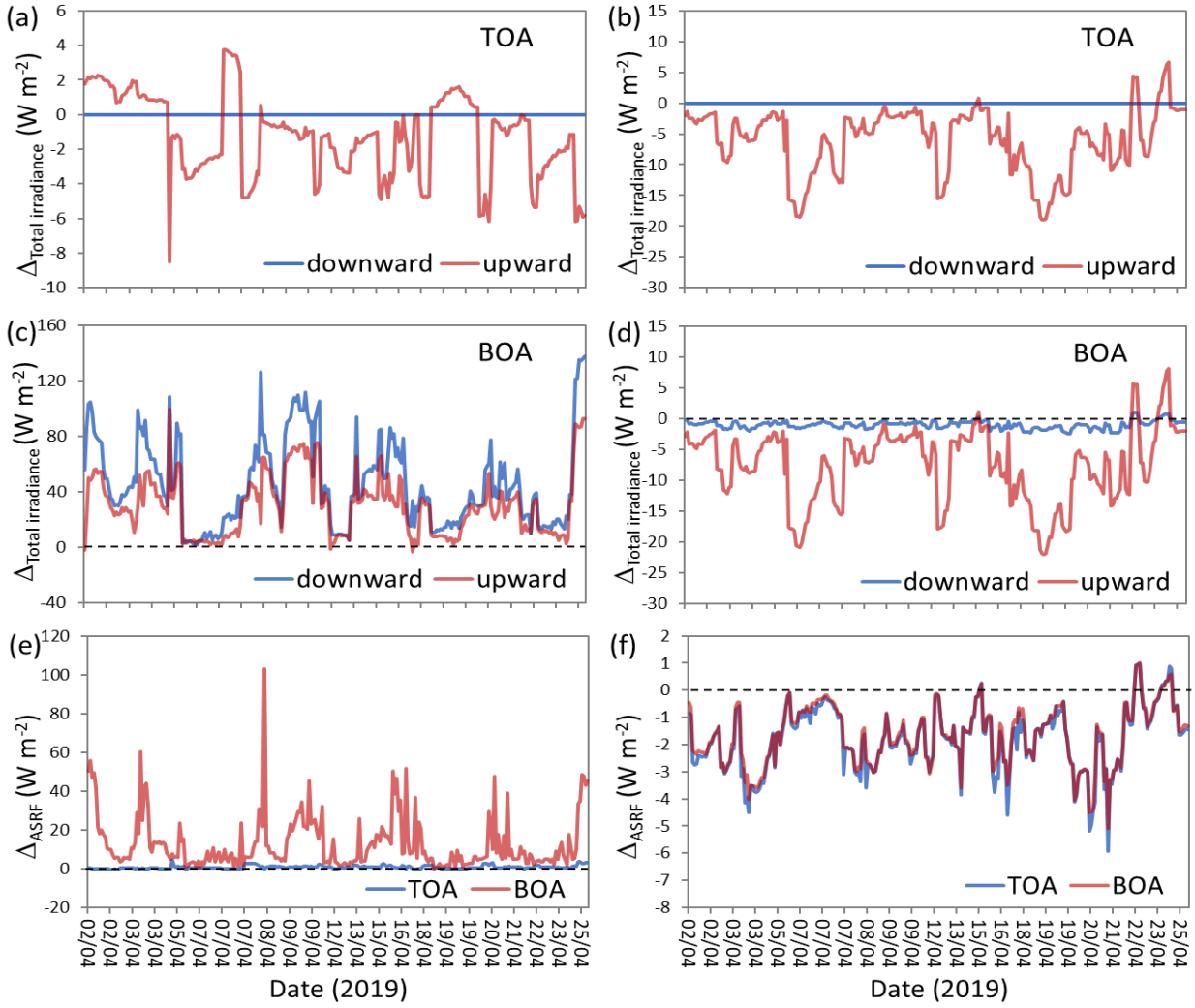

Figure 10: Influences of atmospheric profile (left column) and land surface albedo (right column) on total irradiances and *ASRF*. (a) differences of total downward and upward irradiances (*TDI* and *TUI*) at the TOA between simulations with the pre-defined midlatitude winter profile and user-specified profiles; (b) differences of *TDI* and *TUI* at the TOA between simulations with local noon surface albedo and instantaneous surface albedo; (c) as (a), but for BOA; (d) as (b), but for BOA; (e) differences of *ASRF* between simulations with the pre-defined midlatitude winter profile and user-specified profiles at the TOA and BOA; (f) differences of *ASRF* between simulations with local noon surface albedo and instantaneous surface albedo at the TOA and BOA.

4.3 ~~Comparisons and validation~~ Difference from AERONET products

~~In order to evaluate the results of aerosol radiative forcing comprehensively, we compare the radiative transfer simulations with the AERONET operational products and the WRF-Chem simulations. The downward irradiance at the surface directly measured by high-precision solar radiation monitoring station during the DAO-K campaign are further adopted to validate the RT model and WRF-Chem model simulations.~~

~~4.3.1 Comparison between radiative transfer simulations and AERONET results~~

Aerosol radiative forcing at the TOA and BOA are operational products provided routinely by AERONET. Measurements of the CE318-T #1141 during the DAO-K campaign have been processed by AERONET. Therefore, we can compare the *ASRF* product from AERONET with our simulations. For AERONET, broadband upward and downward irradiances in the SW ranges from 0.2 to 4.0 μm were calculated by radiative transfer model with retrieved aerosol properties as model inputs (http://aeronet.gsfc.nasa.gov). However, ~~It should be noted that~~ AERONET adopts different definition of *ASRF* that only taking the downward irradiance at the BOA and the upward irradiance at the TOA into consideration (García et al., 2012). The upward irradiances with and without aerosols in Eq. (2), along with the downward irradiances with and without aerosols in Eq. (1), are not taken into account. Omitting the downward irradiances with and without aerosols in the AERONET definition won't make much difference in~~of~~ *ASRF* at the TOA. But for the *ASRF* at the BOA, it is predictable that neglecting the upward irradiance ~~with and without aerosols in the AERONET definition~~ will lead to obvious difference. Some existing studies have executed this kind of comparison (García et al., 2008; García et al., 2012; Bi et al., 2014) and reported that AERONET trends to overestimate aerosol *ASRF* at the BOA (García et al., 2012).

Fig. 11 presents the correlations of instantaneous aerosol *ASRF* between the RT model simulations and the AERONET products. It is obvious that there are linear relationships between our RT simulations and the AERONET results with R^2 up to 0.98 and 0.99 at the TOA and BOA, respectively. Two *ASRF* results at the TOA show good consistency with a slope of 1.01, even though the calculated SW ranges are not an exact match (i.e., 0.28~3.0 μm for this study, and 0.2~4.0 μm for AERONET). But for BOA, the AERONET products are obvious stronger~~greater~~ than the corresponding RT model simulations (with a slope of 1.24), which ~~is in agreement~~agrees with the conclusion of the previous study (García et al., 2012).

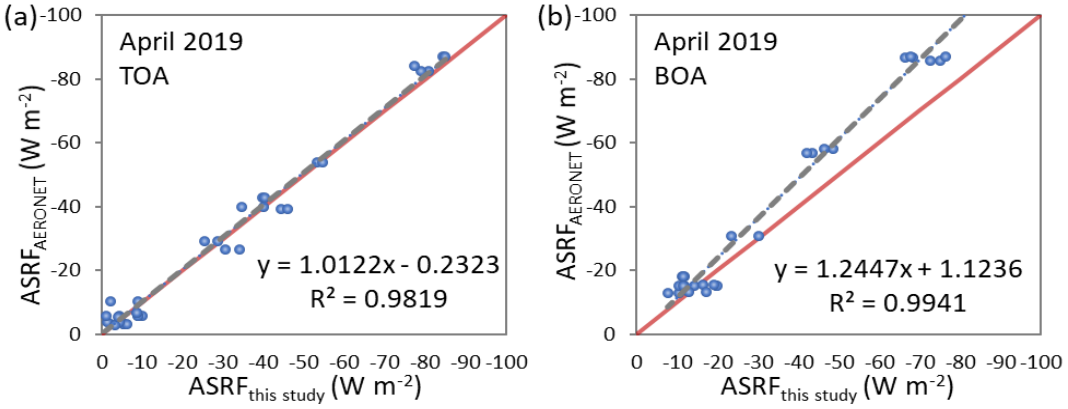

Figure 11: Correlations of instantaneous *ASRF* between radiative transfer (RT) model simulations in this study and the AERONET products ~~at Kashi site~~ during the DAO-K campaign (a) TOA, (b) BOA.

5 Comparison with WRF-Chem simulations

5.1~~4.3.2~~ Comparison between radiative transfer ~~model~~ and WRF-Chem ~~model~~ simulations

Fig. 12 compares the assimilated aerosols to the observations. Evidently, the assimilation greatly improves the particulate matter concentrations and show reasonable variations in accordance with the dust episodes. However, two disadvantages are noticeable. One is the assimilation fails to reproduce the extremely high $PM_{2.5}$ and PM_{10} on 24~25 April 2019, because the background error covariance~~BEC~~ is not specific for the model error in the strong dust storm. A better model result for the specific dust storm requires improving the model capability of simulating dust emission and the transport of dust particulates besides data assimilation. Another is the assimilated *AOD* indeed increases but not well approaches the observations. The reason is that we only assimilated *AOD* by assuming the invariable extinction coefficients. Hence, this low bias in *AOD* cannot be eliminated by choosing a scaling factor smaller than 50 % in the observation error for that it will damage the surface-layer particulate results. As a result, we give a priority to the high quality of the surface-layer aerosol assimilation, and the aerosol optical depth in the assimilated WRF-Chem results is underestimated, which should be kept in mind when comparing the WRF-Chem results with the RT model simulations.

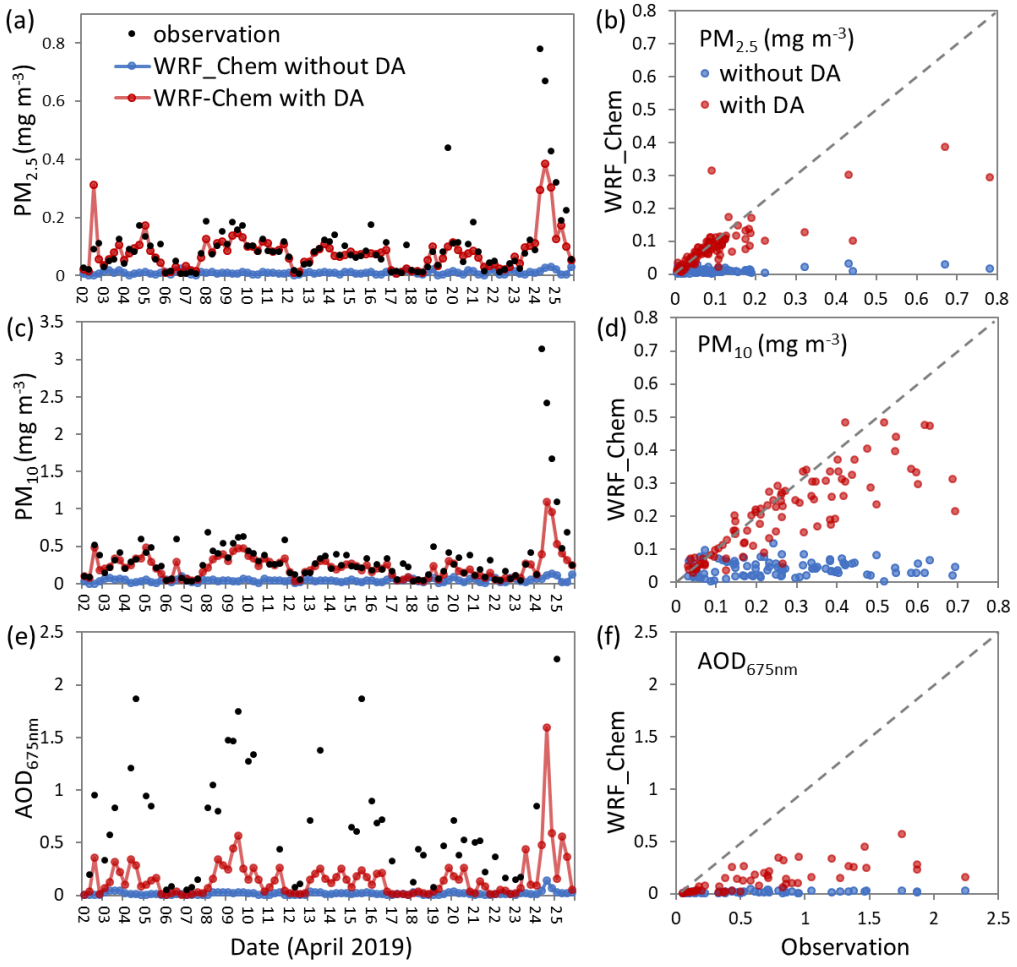

Figure 12: Comparisons of the surface-layer $PM_{2.5}$ (a, b), PM_{10} (c, d) concentrations and *AOD* at 675 nm (e, f) among the observations, the WRF-Chem simulations with and without data assimilations (DA) in April 2019. The observations have been interpolated to 0:00, 6:00, 12:00, 18:00 UTC of each day.

Fig. 13 illustrates the results of daily mean *ASRF*s during DAO-K campaign simulated by the SBDART radiative transfer and WRF-Chem models. Two results show similar variation patterns. However, it is notable that the WRF-Chem results are significantly stronger~~greater~~ than which of RT simulations in dust-polluted cases on 9, 24, and 25 April 2019. According to RT simulations, the strongest radiative forcing occurred on 25 April 2019. However, the most significant *ASRF* of WRF-Chem simulation is found on 24 April 2019 followed by 25 April 2019. As mentioned above, heavy dust storms broke out on these two days during the DAO-K campaign. The extreme values of daily mean *ASRF* calculated by RT model are -46 W m^{-2} at the TOA, 48 W m^{-2} in ATM, and -94 W m^{-2} at the BOA~~, b~~. But with respect to the WRF-Chem simulations, the corresponding values are -78, 101, and -178 W m^{-2}, respectively. The significant differences between the two kinds of simulated results in dust cases should be further evaluated.

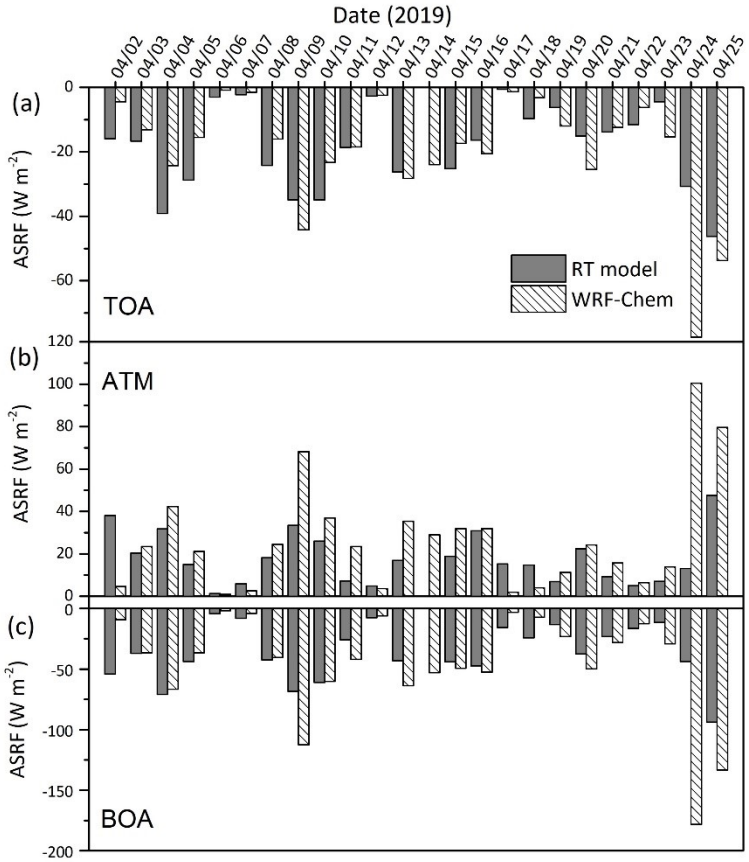

Figure 13: Comparisons of daily mean *ASRF* between the RT model calculations and the WRF-Chem simulations at Kashi site during the DAO-K campaign ~~(upper panel~~(a) TOA; ~~middle panel:~~ (b) ATM; ~~lower panel:~~ (c) BOA).

5.2~~4.3.3~~ Validation by ground-based irradiance measurements

Fig. 14 directly compares the RT and WRF-Chem simulated downward irradiances at surface with the ground-based measurements under three different sky conditions (i.e., clear case, heavy dust case, and two-layer dust case). The RT simulations of total, direct, and diffuse downward irradiances in the three situations agree well with high-precision measurements of pyrheliometer and pyranometers. The percent differences of RT-simulated total irradiance with respect to the measurements are only 0.03 % for the clear case, -2.67 % for the heavy dust case, and -0.43 % for the two-layer dust case. Except for the heavy dust case, they are within the pyranometer measurement uncertainties (0.66 %). As for the WRF-Chem simulations, the total irradiances in the clear sky case are consistent with RT simulations and measurements (Fig. 14a). But for the direct irradiances, there are obvious differences between the WRF-Chem simulations and the corresponding measurements (Fig. 14b). Moreover, the WRF-Chem simulated diffuse irradiances in the clear case (Fig. 14c), the total, direct, and diffuse irradiances in the heavy dust and two-layer dust cases (Fig. 14d~i) are significantly distinct from the measurements and RT simulations.

One of the most noticeable features in the curves of WRF-Chem results is the sudden jump around 6:00 UTC, which can be attributed to data assimilations restarted at 6:00 UTC and ran to the next analysis time 12:00 UTC. The WRF-Chem results are greatly improved after 6:00 UTC in the dust-polluted cases. It is evident that data assimilations at 6:00 UTC can ameliorate the WRF-Chem simulations in dust cases, but the correction effects are still limited. So, the problems of the WRF-Chem simulation have not yet been fully resolved by the assimilations of aerosol optical depth and particulate matter concentrations. This conclusion is in accordance with Figs. 12 and 13. Our measurements have proved that the simulations of RT model are reliable in both of clear and high aerosol loading situations. The WRF-Chem model preforms better in clear sky than in the dust-polluted conditions. There is still room for improving the WRF-Chem simulation of dust aerosol radiative forcing.

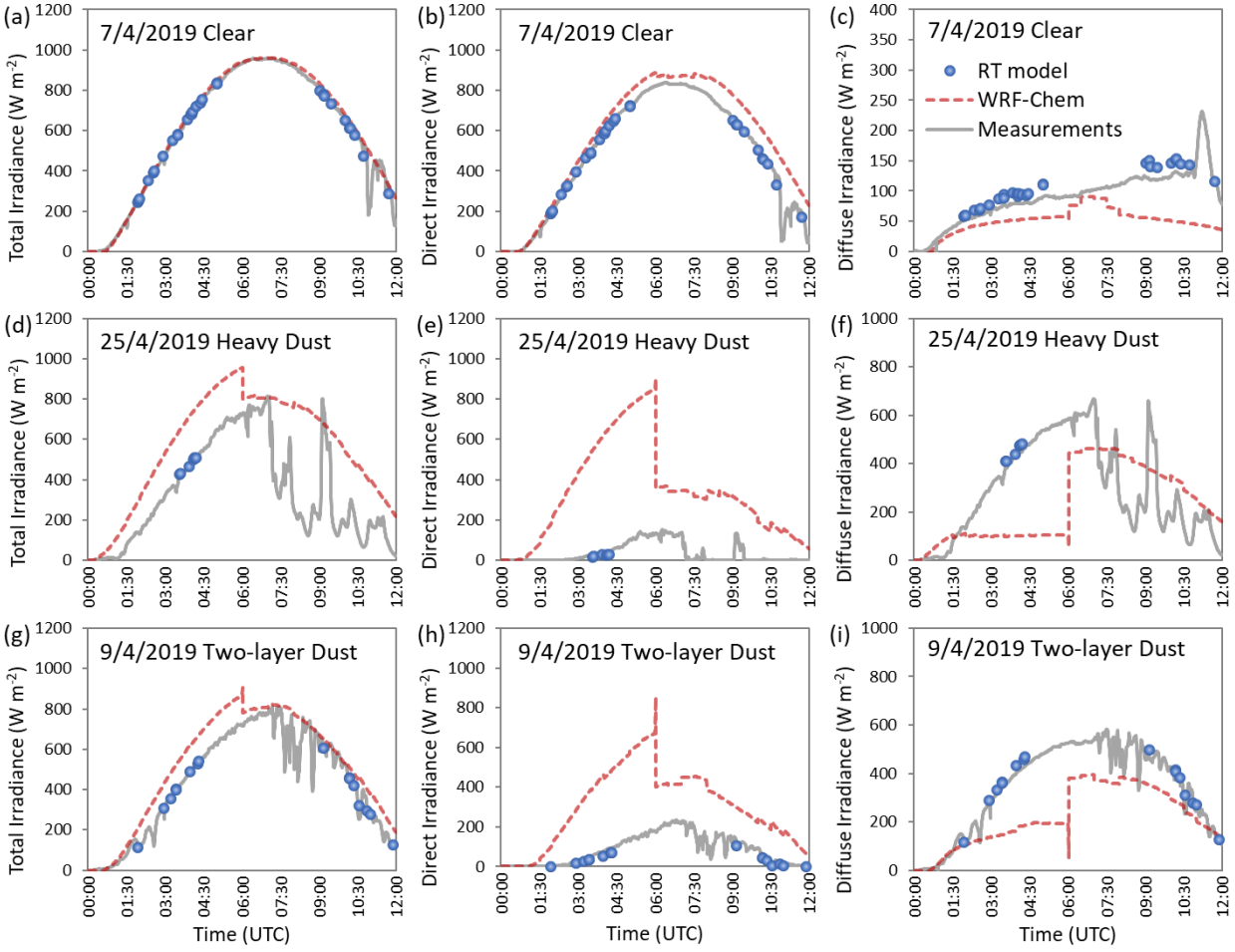

Figure 14: Comparisons of total, direct and diffuse downward irradiances at the bottom of atmosphere for the clear case (upper three panels), the heavy dust case (middle three panels), and the two-layer dust case (lower three panels) at Kashi site (blue points: simulated by the RT model; red dash lines: simulated by the WRF-Chem model with data assimilations at 0:00 and 6:00 UTC; gray solid lines: measured by pyrheliometer and pyranometers).

6~~5~~ Summary and conclusions

Dust aerosol particles play an important role in local and global climate changes by influencing the solar radiation budget through scattering and absorbing processes, especially for the region close to dust sources such as deserts. The complicated scattering and absorption characteristics of dust particles make it challenging to estimate their direct radiative forcing. Therefore, the Dust Aerosol Observation-Kashi (DAO-K) campaign was designed and preformed near the Taklimakan D~~d~~esert, ~~that is~~ which represents a substantial and stable source of Asian dust aerosol particles. For almost one month, comprehensive observations of aerosol properties (i.e., aerosol optical depth, Ångström exponent, single scattering albedo, and asymmetry factor), atmospheric profiles (including ozone ~~profiles~~ measurements), and land surface properties were obtained by a variety of ground-based and satellite ~~apparatus~~ instruments in the dust ~~borne~~ season, and were applied to estimate the ~~in~~ aerosol solar radiative forcing ~~analysis~~ using the SBDART radiative transfer model ~~simulations~~. In addition to high-quality dataset of volume aerosol properties satisfying the AERONET and SONET level 1.5 data criteria, the daily specified atmospheric profiles and diurnal variations of ~~land~~ surface albedo were also considered ~~in detail~~ in the ~~simulations~~calculations. The simulated results show that the average values of daily mean *ASRF* at Kashi are -19 W m^{-2} at the TOA and -36 W m^{-2} at the BOA during the DAO-K campaign. The dust-dominant aerosol particles have stronger cooling effects at both the TOA and BOA~~top and bottom of atmosphere~~, and more significant warming effects in the atmosphere than other low aerosol loading situations. Nevertheless, the radiative forcing efficiencies in dust-polluted cases exhibit lower than those in clear-sky conditions. The average influences of different profiles on *ASRF* are small at the TOA (0.8 W m^{-2}) but remarkable at the BOA (13 W m^{-2}). The cooling effects of aerosol radiative forcing at the BOA will be significantly underestimated by simulations with the pre-defined midlatitude winter profile instead of the user-specified Kashi profiles. Simulations using the local noon albedo trend to overestimate the cooling effects of the aerosol radiative forcing both at the TOA and BOA. Different LAS settings lead to moderate impacts on *ASRF* with average effects of 1.8 W m^{-2} at the TOA and 1.7 W m^{-2} at the BOA.

By assimilating the multi-wavelength ~~volume~~ columnar *AOD* and the surface-based measurements of ~~layer~~ $PM_{2.5}$ and PM_{10} mass concentrations, the aerosol solar radiative forcing was also simulated for the time period of DAO-K field campaign using the WRF-Chem model. ~~The measurements of downward irradiances at the surface were applied in evaluating the two kinds of simulations. By comparison of the daily mean *ASRF*, two results~~The RT and WRF-Chem simulations of the daily mean *ASRF* present similar variation patterns. However, the WRF-Chem results are significantly stronger than the RT simulations in dust-polluted cases. For the heavy dust episode, the percent difference of daily mean *ASRF* between the RT ~~model~~ and the WRF-Chem~~ model~~ simulations are greater than 50 % at the TOA, BOA, and in ATM. The measurements of downward solar irradiances at the surface were applied in evaluating the RT and WRF-Chem simulations. The direct, diffuse (and the sum of both) downward irradiances simulated by RT model in the clear-sky, heavy dust, two-layer dust conditions are all in sufficient~~good~~ agreement with ground-based measurements. As for the WRF-Chem simulations, the total irradiances in the clear sky case are consistent with RT calculations and measurements. But the direct, diffuse, and total irradiances simulated by WRF-Chem significantly deviate from measurements in the dust-polluted situations. Data assimilations can

obvious improve the WRF-Chem simulations in dust cases, but the correction effects are still limited. Based on these findings it is concluded that the SBDART radiative transfer model provides credible estimates of dust particle solar radiative forcing if supplied with reliable model inputs, but the WRF-Chem model is prone to overestimate the radiative forcing effects of dust aerosols. Considering the actual measured atmospheric profiles and diurnal variations of land surface albedo can improve the radiative transfer model simulations. Optimizations of dust emission scheme, background error setting of dust assimilation system, dust parameterization including nonsphericity, are proposed as the promising approaches to improve the WRF-Chem simulations of dust radiative forcing. We would like to emphasize, however, that the comparisons are ~~is~~ only conducted at one site and in a limited time period in this study. Future research on this topic should include a systematic evaluation of RT and WRF-Chem model simulations on larger space and time scales.

Data availability. The MODIS, OMI, and AERONET products can be accessed at https://modis.gsfc.nasa.gov/, https://disc.gsfc.nasa.gov/, and https://aeronet.gsfc.nasa.gov/, respectively (last accessed July 2019).

Competing interests. The authors declare that they have no conflict of interest.

Acknowledgements. This research was funded by the National Natural Science Foundation of China (NSFC), grant number 41871271, and the National Key R&D Program of China, grant number 2016YFE0201400. The authors acknowledge the groups of MODIS, OMI, and AERONET for making the surface albedo, ozone profile, and radiative forcing products available, respectively. We also thank the Kashi regional meteorological bureau and the China National environmental monitoring centre for releasing the data of atmospheric sounding and PM_{10} concentration of Kashi, respectively. The Anhui Yunnengtian Intelligent Technology Co., Ltd., China is acknowledged for providing the All sky view camera and technical support. The first author also wishes to thank Haofei Wang, Thierry Podvin, Igor Veselovskiy, Jie Chen, and Ying Zhang for participating the measurements.

References

Adesina, A. J., Kumar, K. R., Sivakumar, V., and Griffith, D.: Direct radiative forcing of urban aerosols over Pretoria (25.75°S, 28.28°E) using AERONET Sunphotometer data: first scientific results and environmental impact, Journal of Environmental Sciences-china, 26, 2459-2474, doi: 10.1016/j.jes.2014.04.006, 2014.

Ansmann, A., Petzold, A., Kandler, K., Tegen, I., Wendisch, M., Müller, D., Weinzierl, B., Müller, T. and Heintzenberg, J.: Saharan Mineral Dust Experiments SAMUM-1 and SAMUM-2: What have we learned? Tellus, 63B, 403-429. doi:10.1111/j.1600-0889.2011.00555.x, 2011.

Babu, S. S., Satheesh, S. K., and Moorthy, K. K.: Aerosol radiative forcing due to enhanced black carbon at an urban site in India, Geophys. Res. Lett., 29, 27-21, doi:10.1029/2002GL015826, 2002.

Bhartia, P. K., Mcpeters, R. D., Mateer, C. L., Flynn, L. E., and Wellemeyer, C. G.: Algorithm for the estimation of vertical ozone profiles from the backscattered ultraviolet technique, J. Geophys. Res., 101, 18793-18806, doi: 10.1029/96JD01165, 1996.

Bi, J., Huang, J., Hu, Z., Holben, B. N., and Guo, Z.: Investigating the aerosol optical and radiative characteristics of heavy haze episodes in Beijing during January of 2013, J. Geophys. Res. Atmos., 119, 9884-9900, doi: 10.1002/2014JD021757, 2014.

Bi, L., Yang, P., Kattawar, G. W., and Kahn, R.: Modeling optical properties of mineral aerosol particles by using nonsymmetric hexahedra. Appl. Optics, 49(3), 334-342, doi:10.1364/AO.49.000334, 2010.

Bierwirth, E., Wendisch, M., Ehrlich, A., Heese, B., Tesche, M., Althausen, D., Schladitz, A., Müller, D., Otto, S., Trautmann, T., Dinter, T., von Hoyningen-Huene, W., and Kahn, R.: Spectral surface albedo over Morocco and its impact on radiative forcing of Saharan dust. Tellus, 61B, 252-269, DOI: 10.1111/j.1600-0889.2008.00395.x, 2009.

Bory, A. J., Biscaye, P. E., and Grousset, F. E.: Two distinct seasonal Asian source regions for mineral dust deposited in Greenland (NorthGRIP), Geophys. Res. Lett., 30, 1167, doi:10.1029/2002GL016446, 2003.

Chen, S., Huang, J., Zhao, C., Qian, Y., Leung, L. R., and Yang, B.: Modeling the transport and radiative forcing of Taklimakan dust over the Tibetan Plateau: A case study in the summer of 2006, J. Geophys. Res. Atmos., 118, 797-812, doi:10.1002/jgrd.50122, 2013.

Chen, S., Zhao, C., Qian, Y., Leung, L. R., Huang, J., Huang, Z., Bi, J., Zhang, Y., Shi, J., Yang, L., Li, D., and Li, J.: Regional modeling of dust mass balance and radiative forcing over East Asia using WRF-Chem, Aeolian Research, 15, 15-30, http://dx.doi.org/10.1016/j.aeolia.2014.02.001, 2014.

Chen, S., Huang, J., Li, J., Jia, R., Jiang, N., Kang, L., Ma, X., and Xie, T.: Comparison of dust emissions, transport, and deposition between the Taklimakan Desert and Gobi Desert from 2007 to 2011. Science China Earth Sciences, 60(1), 1338-1355, doi:10.1007/s11430-016-9051-0, 2017.

Chen, S., Yuan, T., Zhang, X., Zhang, G., Feng, T., Zhao, D., Zang, Z., Liao, S., Ma, X., Jiang, N., Zhang, J., Yang, F., and Lu, H.: Dust modeling over East Asia during the summer of 2010 using the WRF-Chem model, J. Quant. Spectrosc. Radiat. Transfer, 213, 1-12, https://doi.org/10.1016/j.jqsrt.2018.04.013, 2018.

China Meteorological Administration, Operational specifications for conventional upper-air meteorological observations, China Meteorological Press, Beijing, China, 2010.

Dubovik, O., Sinyuk, A., Lapyonok, T., Holben, B. N., Mishchenko, M., Yang, P., Eck, T. F., Volten, H., Munõz, O., Veihelmann, B., van der Zande, W. J., Leon, J. F., Sorokin, M., and Slutsker, I.: Application of spheroid models to account for aerosol particle nonsphericity in remote sensing of desert dust, J. Geophys. Res., 111, doi:10.1029/2005JD006619, 2006.

Esteve, A. R., Estelles, V., Utrillas, M. P., and Martinezlozano, J. A.: Analysis of the aerosol radiative forcing over a Mediterranean urban coastal site, Atmospheric Research, 137, 195-204, doi: 10.1016/j.atmosres.2013.10.009, 2014.

Fast, J. D., Gustafson Jr., W. I., Easter, R. C., Zaveri, R. A., Barnard, J. C., Chapman, E. G., Grell, G. A., and Peckham, S. E.: Evolution of ozone, particulates, and aerosol direct ra- diative forcing in the vicinity of Houston using a fully coupled meteorology–chemistry–aerosol model, J. Geophys. Res., 111, D21305, doi:10.1029/2005JD006721, 2006.

García, O. E., Díaz, A. M., Expósito, F. J., Díaz, J. P., Dubovik, O., Dubuisson, P., Roger, J. C., Eck, T. F., Sinyuk, A., Derimian, Y., Dutton, E. G., Schafer, J. S., Holben, B. N., and García, C. A.: Validation of AERONET estimates of atmospheric solar fluxes and aerosol radiative forcing by ground-based broadband measurements, J. Geophys. Res. Atmos., 113, 6089-6098, doi:10.1029/2008JD010211, 2008.

García, O. E., Díaz, J. P., Expósito, F. J., Díaz, A. M., Dubovik, O., Derimian, Y., Dubuisson, P., and Roger, J. C.: Shortwave radiative forcing and efficiency of key aerosol types using AERONET data, Atmos. Chem. Phys., 12, 5129-5145, doi:10.5194/acp-12-5129-2012, 2012.

Ginoux, P., Chin, M., Tegen, I., Prospero, J. M., Holben, B., Dubovik, O., and Lin, S. J.: Sources and distributions of dust aerosols simulated with the GOCART model, J. Geophys. Res.,106(D17), 20255-20273, 2001.

Grell, G. A., Peckham, S. E., Schmitz, R., McKeen, S. A., Frost, G., Skamarock, W. C., and Eder, B.: Fully coupled ‘‘online’’ chemistry within the WRF model, Atmos. Environ., 39, 6957– 6975, doi:10.1016/j.atmosenv.2005.04.027, 2005.

Guenther, A., Karl, T., Harley, P., Wiedinmyer, C., Palmer, P. I., and Geron, C.: Estimates of global terrestrial isoprene emissions using MEGAN (Model of Emissions of Gases and Aerosols from Nature), Atmos. Chem. Phys., 6, 3181-3210, 2006.

Holben, B. N., Eck, T. F., Slutsker, I., Tanré, D., Buis, J. P., Setzer, A., Vermote, E., Reagan, J. A., Kaufman, Y. J., Nakajima, T., Lavenu, F., Jankowiak, I., and Smirnov, A.: AERONET—A Federated Instrument Network and Data Archive for Aerosol Characterization, Remote Sens. Environ., 66, 1-16, 1998.

Hu, Q., Goloub, P., Veselovskii, I., Bravo-Aranda, J., Popovici, I. E., Podvin, T., Haeffelin, M., Lopatin, A., Dubovik, O., Pietras, C., Huang, X., Torres, B., and Chen, C.: Long-range-transported Canadian smoke plumes in the lower stratosphere over northern France, Atmos. Chem. Phys., 19, 1173–1193, https://doi.org/10.5194/acp-19-1173-2019, 2019.

Huang, J., Fu, Q., Su, J., Tang, Q., Minnis, P., Hu, Y., Yi, Y. and Zhao, Q.: Taklimakan dust aerosol radiative heating derived from CALIPSO observations using the Fu-Liou radiation model with CERES constraints, Atmos. Chem. Phys., 9, 4011-4021, doi:10.5194/acp-9-4011-2009, 2009.

Huang, J., Wang, T., Wang, W., Li, Z., and Yan, H.: Climate effects of dust aerosols over East Asian arid and semiarid regions, J. Geophys. Res. Atmos., 119, doi:10.1002/2014JD021796, 2014.

Intergovernmental Panel on Climate Change (IPCC): Climate change 2007: the physical science basis. Contribution of Working Group I to the Fourth Assessment Report of the Intergovernmental Panel on Climate Change, Cambridge University Press, Cambridge, United Kingdom and New York, USA, 2007.

Jäkel, E., Wendisch, M., and Mayer, B.: Influence of spatial heterogeneity of local surface albedo on the area-averaged surface albedo retrieved from airborne irradiance measurements. Atmos. Meas. Tech., 6, 527-537, doi:10.5194/amtd-6-527-2013, 2013.

Kaskaoutis, D. G., Kambezidis, H. D., Hatzianastassiou, N., Kosmopoulos, P. G., and Badarinath, K. V. S.: Aerosol climatology: dependence of the Angstrom exponent on wavelength over four AERONET sites. Atmos. Chem. Phys. Discuss., 7, 7347–7397, 2007.

Kleist, D. T., Parish, D. F., Derber, J. C., Treadon, R., Wu, W. S., and Lord, S.: Introduction of the GSI into the NCEP global data assimilation system, Weather Forecast, 24, 1691-1705, 2009.

Lenoble, J., Remer, L., and Tanré, D.: Aerosol Remote Sensing, Springer Berlin Heidelberg, doi:10.1007/978-3-642-17725-5, 2013.

Lewis, P. and Barnsley, M. J.: Influence of the sky radiance distribution on various formulations of the earth surface albedo, Proc. Conf. Phys. Meas. Sign. Remote Sen. Val d'Isere, France, 707–715, 1994.

~~Li, L., Li, Z., Li, K., Blarel, L., and Wendisch, M.: A method to calculate Stokes parameters and angle of polarization of skylight from polarized CIMEL sun/sky radiometers, J. Quant. Spectrosc. Radiat. Transfer, 149, 334-346, http://dx.doi.org/10.1016/j.jqsrt.2014.09.003, 2014.~~

Li, L., Li, Z., Dubovik, O., Zheng, X., Li, Z., Ma, J., and Wendisch, M.: Effects of the shape distribution of aerosol particles on their volumetric scattering properties and the radiative transfer through the atmosphere that includes polarization. Applied Optics, 58(6), 1475-1484, doi:10.1364/AO.58.001475, 2019.

Li, R., Dong, X., Guo, J., Fu, Y., Zhao, C., Wang, Y., and Min, Q.: The implications of dust ice nuclei effect on cloud top temperature in a complex mesoscale convective system, Sci Rep, 7, 13826, https://doi.org/10.1038/s41598-017-12681-0, 2017.

Li, Z., Blarel, L., Podvin, T., Goloub, P., Buis, J. P., and Morel, J. P.: Transferring the calibration of direct solar irradiance to diffuse-sky radiance measurements for CIMEL Sun-sky radiometers, Appl. Opt., 47, 1368–1377, https://doi.org/10.1364/AO.47.001368, 2008.

~~Li, Z., Li, D., Li, K., Xu, H., Cheng, X., Chen, C., Xie, Y., Li, L., Li, L., Li, W., Lv, Y., Qie, L., Zhang, Y., and Gu, X.: Sun/sky radiometer observation network with the extension of multi-wavelength polarization measurements, Journal of Remote Sensing, 19, 496-520, doi:10.11834/jrs.20144129, 2015.~~

Li, Z. Q., Xu, H., Li, K. T., Li, D. H., Xie, Y. S., Li, L., Zhang, Y., Gu, X. F., Zhao, W., Tian, Q. J., Deng, R. R., Su, X. L., Huang, B., Qiao, Y. L., Cui, W. Y., Hu, Y., Gong, C. L., Wang, Y. Q., Wang, X. F., Wang, J. P., Du, W. B., Pan, Z. Q., Li, Z. Z., and Bu, D.: Comprehensive Study of Optical, Physical, Chemical, and Radiative Properties of Total Columnar Atmospheric Aerosols over China: An Overview of Sun-Sky Radiometer Observation Network (SONET) Measurements, Bulletin of the American Meteorological Society, 99, 739-755, doi:10.1175/BAMS-D-17-0133.1, 2018.

Liang, S.: Quantitative Remote Sensing of Land Surfaces, John Wiley, Hoboken, 2004.

Liu, L., Guo, J., Gong, H., Li, Z., Chen, W., Wu, R., Wang, L., Xu, H., Li, J., Chen, D., and Zhai, P.: Contrasting Influence of Gobi and Taklimakan Deserts on the Dust Aerosols in Western North America. Geophysical Research Letters, 46(15), 9064-9071, doi:10.1029/2019GL083508, 2019.

Liu, Z., Liu, D., Huang, J., Vaughan, M., Uno, I., Sugimoto, N., Kittaka, C., Trepte, C., Wang, Z., Hostetler, C., and Winker, D.: Airborne dust distributions over the Tibetan Plateau and surrounding areas derived from the first year of CALIPSO lidar observations, Atmos. Chem. Phys., 8, 5045–5060, doi:10.5194/acp-8-5045-2008, 2008.

Liu, Z., Liu, Q., Lin, H. C., Schwartz, C. S., Lee, Y. H., and Wang, T.: Three-dimensional variational assimilation of MODIS aerosol optical depth: implementation and application to a dust storm over East Asia, J. Geophys. Res., 116, D23206, doi:10.1029/2011JD016159, 2011a.

Liu, J., Zheng, Y., Li, Z., Flynn, C., Welton, E. J., and Cribb, M.: Transport, vertical structure and radiative properties of dust events in southeast China determined from ground and space sensors, Atmospheric Environment, 45(35), 6469-6480, doi:10.1016/j.atmosenv.2011.04.031, 2011b.

Lucht, W., Schaaf, C. B., and Strahler, A. H.: An algorithm for the retrieval of albedo from space using semiempirical BRDF models, IEEE Trans. Geosci. Remote Sens., 38, 977-998, 2000.

Mikami, M., Shi, G., Uno, I., Yabuki, S., Iwasaka, Y., Yasui, M., Aoki, T., Tanaka, T.Y., Kurosaki, Y., Masuda, K., Uchiyama, A., Matsuki, A., Sakai, T., Takemi, T., Nakawo, M., Seino, N., Ishizuka, M., Satake, S., Fujita, K., Hara, Y., Kai, K., Kanayama, S., Hayashi, M., Du, M., Kanai, Y., Yamada, Y., Zhang, X.Y., Shen, Z., Zhou, H., Abe, O., Nagai, T., Tsutsumi, Y., Chiba, M., and Suzuki, J.: Aeolian dust experiment on climate impact: An overview of Japan-China joint project ADEC, Global and Planetary Change, 52, 142-172, doi:10.1016/j.gloplacha.2006.03.001, 2006.

Minnis, P., Mayor, S., Smith, W. L., and Young, D. F.: Asymmetry in the diurnal variation of surface albedo, IEEE Trans. Geosci. Remote Sens., 35, 879–891, doi:10.1109/36.602530, 1997.

Otto, S., de Reus, M., Trautmann, T., Thomas, A., Wendisch, M., and Borrmann, S.: Atmospheric radiative effects of an in-situ measured Saharan dust plume and the role of large particles. Atmos. Chem. Phys., 7, 4887-4903, 2007.

Parrish, D. F., and Derber, J. C.: The National Meteorological Center's spectral statistical interpolation analysis system, Mon. Weather Rev., 120, 1747-1763, doi:10.1175/1520-0493(1992)120<1747:TNMCSS>2.0.CO;2, 1992.

Ricchiazzi, P., Yang, S., Gautier, C., and Sowle, D.: SBDART: A Research and Teaching Software Tool for Plane-Parallel Radiative Transfer in the Earth's Atmosphere, Bulletin of the American Meteorological Society, 79, 2101-2114, 1998.

Schaaf, C. B., Gao, F., Strahler, A. H., Lucht, W., Li, X., Tsang, T., Strugnell, N. C., Zhang, X., Jin, Y., Muller, J. P., Lewis, P., Barnsley, M., Hobson, P., Disney, M., Roberts, G., Dunderdale, M., Doll, C., d'Entremont, R. P., Hu, B., Liang, S., Privette, J. L., and Roy, D.: First operational BRDF, albedo nadir reflectance products from MODIS, Remote Sensing of Environment, 83, 135-148, 2002.

Schaaf C., and Wang Z.: MCD43A1 MODIS/Terra+Aqua BRDF/Albedo Model Parameters Daily L3 Global - 500m V006, NASA EOSDIS Land Processes DAAC, http://doi.org/10.5067/MODIS/MCD43A1.006, 2015.

Schwartz, C. S., Liu, Z., Lin, H. C., and McKeen, S. A.: Simultaneous three-dimensional variational assimilation of surface fine particulate matter and MODIS aerosol optical depth, J. Geophys. Res., 117, D13202, doi:10.1029/2011JD017383, 2012.

Stapf, J., Ehrlich, A., Jäkel, E., Lüpkes, C., and Wendisch, M.: Reassessment of the common concept to derive the surface cloud radiative forcing in the Arctic: Consideration of surface albedo-cloud interactions, Atmos. Chem. Phys. Discuss., https://doi.org/10.5194/acp-2019-534, in review, 2019.

Sun, H., Pan, Z., and Liu, X.: Numerical simulation of spatial-temporal distribution of dust aerosol and its direct radiative effects on East Asian climate. J. Geophys. Res., 117, doi:10.1029/2011JD017219, 2012.

Tegen, I., Bierwirth, E., Heinold, B., Helmert, J., and Wendisch M.: The effect of measured surface albedo on modeled Saharan dust radiative forcing. J. Geophys. Res., 115, D24312, doi:10.1029/2009JD013764, 2009.

Twomey, S.: The Influence of Pollution on the Shortwave Albedo of Clouds, J. Atmos. Sci., 34, 1149-1152, 1977.

Valenzuela, A., Olmo, F. J., Lyamani, H., Anton, M., Quirantes, A., and Alados-Arboledas, L.: Aerosol radiative forcing during African desert dust events (2005–2010) over Southeastern Spain, Atmos. Chem. Phys., 12, 10331-10351, doi:10.5194/acp-12-10331-2012, 2012.

Veselovskii, I., Goloub, P., Podvin, T., Bovchaliuk, V., Derimian, Y., Augustin, P., Fourmentin, M., Tanre, D., Korenskiy, M., Whiteman, D. N., Diallo, A., Ndiaye, T., Kolgotin, A., and Dubovik, O.: Retrieval of optical and physical properties of African dust from multiwavelength Raman lidar measurements during the SHADOW campaign in Senegal, Atmos. Chem. Phys., 16, 7013-7028, doi:10.5194/acp-16-7013-2016, 2016.

Veselovskii, I., Goloub, P., Podvin, T., Tanre, D., Silva, A. D., Colarco, P. R., Castellanos, P., Korenskiy, M., Hu, Q., Whiteman, D. N., Pérez-Ramírez, D., Augustin, P., Fourmentin, M., and Kolgotin, A.: Characterization of smoke and dust episode over West Africa: comparison of MERRA-2 modeling with multiwavelength Mie–Raman lidar observations, Atmos. Meas. Tech., 11, 949-969, https://doi.org/10.5194/amt-11-949-2018, 2018.

Wang, D., Liang, S., He, T., Yu, Y., Schaaf, C. and Wang, Z.: Estimating daily mean land surface albedo from MODIS data, J. Geophys. Res. Atmos., 120, 4825-4841, doi:10.1002/2015JD023178, 2015.

Waquet, F., Peers, F., Ducos, F., Goloub, P., Platnick, S., Riedi, J., Tanré, D., and Thieuleux, F.: Global analysis of aerosol properties above clouds, Geophysical Research Letters, 40(21), 5809-5814, doi:10.1002/2013GL057482, 2013.

Wendisch, M., Hellmuth, O. , Ansmann, A., Heintzenberg, J., Engelmann, R., Althausen, D., Eichler, H., Müller, D., Hu, M., Zhang, Y. and Mao, J.: Radiative and dynamic effects of absorbing aerosol particles over the Pearl River Delta, China. Atmos. Environ., 42, 6405-6416, doi:10.1016/j.atmosenv.2008.02.033, 2008.

Werner, F., Ditas, F., Siebert, H., Simmel, M., Wehner, B., Pilewskie, P., Schmeissner, T., Shaw, R. A., Hartmann, S., Wex, H., Roberts, G. C., and Wendisch, M.: Twomey effect observed from collocated microphysical and remote sensing measurements over shallow cumulus, J. Geophys. Res., 119, 1534-1545, doi:10.1002/2013JD020131, 2014.

Wu, W.S., Purser, R. J., and Parrish, D. F.: Three-dimensional variational analysis with spatially inhomogeneous covariances, Mon. Weather Rev., 130, 2905-2916, doi: 10.1175/1520-0493(2002)130<2905:TDVAWS>2.0.CO;2, 2002.

Xia, X., and Zong, X.: Shortwave versus longwave direct radiative forcing by Taklimakan dust aerosols, Geophysical Research Letters, 36(7), L07803, doi:10.1029/2009GL037237, 2009.

Xu, H., Guo, J., Wang, Y., Zhao, C., Zhang, Z., Min, M., Miao, Y., Liu, H., He, J., Zhou, S., and Zhai, P: Warming effect of dust aerosols modulated by overlapping clouds below, Atmospheric Environment, 166, 393-402, http://dx.doi.org/10.1016/j.atmosenv.2017.07.036, 2017.

Yuan, T., Chen, S., Huang, J., Wu, D., Lu, H., Zhang, G., Ma, X., Chen, Z., Luo, Y., and Ma, X.: Influence of Dynamic and Thermal Forcing on the Meridional Transport of Taklimakan Desert Dust in Spring and Summer. Journal of Climate, 32(3), 749-767, DOI: 10.1175/JCLI-D-18-0361.1, 2019.

Zaveri, R. A., and Peters, L. K.: A new lumped structure photochemical mechanism for large-scale applications, J. Geophys. Res., 104, 30,387-30,415, doi: 10.1029/1999JD900876, 1999.

Zaveri, R. A., Easter, R. C., Fast, J. D., and Peters, L. K.: Model for Simulating Aerosol Interactions and Chemistry (MOSAIC), J. Geophys. Res., 113, D13204, doi:10.1029/2007JD008782, 2008.

Zhao, C., Liu, X., Leung, L. R., Johnson, B., Mcfarlane, S. A., Gustafson, W. I., Fast, J. D., and Easter, R. C.: The spatial distribution of mineral dust and its shortwave radiative forcing over North Africa: modeling sensitivities to dust emissions and aerosol size treatments, Atmos. Chem. Phys., 10, 8821-8838, doi:10.5194/acp-10-8821-2010, 2010.